JOURNAL OF PETROLOGY | VOLUME 53 | NUMBER 8 | PAGES 1569–1596 | 2012 | doi:10.1093/petrology/egs026

Depleted Basaltic Lavas from the Proto-Iceland Plume, Central East Greenland

TOD E. WAIGHT[1]* AND JOEL A. BAKER[2]

[1]INSTITUTE OF GEOGRAPHY AND GEOLOGY, ØSTER VOLDGADE 10, 1350 COPENHAGEN K, DENMARK

[2]SCHOOL OF GEOGRAPHY, ENVIRONMENT AND EARTH SCIENCES, VICTORIA UNIVERSITY OF WELLINGTON, P.O. BOX 600, WELLINGTON, NEW ZEALAND

RECEIVED AUGUST 24, 2011; ACCEPTED MARCH 9, 2012
ADVANCE ACCESS PUBLICATION APRIL 26, 2012

New geochemical and isotopic data are presented for volumetrically minor, depleted low-Ti basalts that occur in the Plateau Basalt succession of central East Greenland (CEG), formed during the initial stages of opening of the North Atlantic at 55 Ma. The basalts have mid-ocean ridge basalt (MORB)-like geochemistry (e.g. depleted light rare earth elements) and are distinct from the high-Ti lavas that dominate the sequence. Rare earth element geochemistry implies derivation from a source more depleted than the typical MORB source, and suggests polybaric melting and contributions from both spinel- and garnet-facies mantle. The low-Ti basalts have Sr–Nd–Pb–Hf isotopic characteristics that are similar to those of depleted magmas from Iceland (e.g. Theistareykir) and adjacent ridges (Kolbeinsey and Reykjanes) and distinct from global MORB (e.g. negative $\Delta^{207}Pb$, and Hf and Nd isotope compositions that plot above the mantle reference line). Isotope and trace element data indicate the involvement of two depleted source components. One component has isotopic compositions similar to other depleted components identified in the North Atlantic and has high Rb/Zr and Ba/Nb. The second is isotopically less depleted with lower Rb/Zr and Ba/Nb. Small degrees of crustal contamination (<1%) by both amphibolitic and granulitic crust result in relatively large changes in isotopic composition (c. 1% lower for $^{206}Pb/^{204}Pb$ and 0·1% higher for $^{87}Sr/^{86}Sr$ depending on the contaminant). Negative ΔNb suggests a MORB affinity for the low-Ti magmas; however, they are distinguished from global normal (N)-MORB on the basis of vertical deviations from the Northern Hemisphere Reference Line (negative $\Delta^{207}Pb$ and positive $\Delta^{208}Pb$), and relative enrichments in Ba, Sr and Pb. The isotopic compositions of the low-Ti CEG basalts suggest correlation with modern depleted components beneath Iceland and adjacent ridges, considered to be derived from upper mantle sources polluted by the Iceland plume. However, small positive Pb peaks when normalized to MORB, and lower Nb distinguish the CEG low-Ti basalts from depleted Icelandic compositions. The lower ΔNb (< 0) and $^{87}Sr/^{86}Sr$, and suggestion of higher $^{206}Pb/^{204}Pb$ in crustally uncontaminated parental melts imply a closer affinity to compositions from the oceanic ridges surrounding Iceland (especially the Reykjanes Ridge), yet they are subtly distinct on the basis of available trace element data. We suggest that this depleted component was an integral part of the plume that melted primarily during the rapid lithospheric uplift and extension associated with continental break-up.

KEY WORDS: *geochemistry; Greenland; Iceland plume; North Atlantic; radiogenic isotopes*

INTRODUCTION

The origin of depleted magmas at hotspots is controversial. One school of thought argues that they are derived from an integral part of the mantle plume and potentially related to a recycled oceanic crust component (e.g. Chauvel & Hémond, 2000; Hoernle *et al.*, 2000; Kempton *et al.*, 2000; Skovgaard *et al.*, 2001; Thirlwall *et al.*, 2004; Frey *et al.*, 2005; Kokfelt *et al.*, 2006). Other workers have argued that the depleted component represents incorporation of the surrounding upper mantle into the plume (e.g. Hanan & Schilling, 1997; Hanan *et al.*, 2000; Blichert-Toft & White, 2001; Stracke *et al.*, 2003). The longevity (~60 Myr) and variability of magmatism associated with the Iceland plume offers an unparalleled opportunity to investigate compositional variations in a mantle plume system over time. The origin of both depleted and enriched components in modern Icelandic volcanism has been

*Corresponding author. E-mail: todw@geo.ku.dk

extensively studied and discussed (e.g. Chauvel & Hémond, 2000; Hanan *et al.*, 2000; Fitton *et al.*, 2003; Stracke *et al.*, 2003; Thirlwall *et al.*, 2004; Kokfelt *et al.*, 2006; Peate *et al.*, 2010). We focus here on magmatism generated in central East Greenland (CEG) during the early activity of the Iceland plume associated with the initial opening of the North Atlantic Ocean at ~55 Ma.

A well-exposed sequence of flood basalts in the Blosseville Coast region has been thoroughly characterized (e.g. Larsen *et al.*, 1989) and correlated with contemporaneous magmatism on the Faroe Islands (e.g. Larsen *et al.*, 1999). This CEG flood basalt sequence is dominated by a suite of magmas derived from relatively enriched mantle sources; these have been the subject of a number of detailed studies investigating their petrogenesis and making comparisons with modern Icelandic basalt compositions (e.g. Tegner *et al.*, 1998*a*; Barker *et al.*, 2006). In this contribution, we focus on a suite of the less studied, volumetrically minor, depleted lavas within the succession that suggest the presence of distinct mantle source components during magmatism. We use detailed, high-quality radiogenic isotope and trace element data to assess their origin and relationship to both the more enriched compositions in the plateau basalts of CEG and the modern depleted mantle components sampled beneath Iceland and adjacent oceanic ridges. Our main conclusion is that these depleted lavas were derived by melting of depleted components that were integral parts of the proto-Iceland plume and that they are similar to, but subtly distinct from, the depleted components currently tapped during magmatism under Iceland and adjacent oceanic ridges.

GEOLOGICAL BACKGROUND

Magmatism in the North Atlantic Igneous Province (NAIP) was initiated over a relatively large area following initial impact of the Iceland plume on the base of the lithosphere at ~60 Ma (e.g. Saunders *et al.*, 1997). Volcanism in CEG has recently been reviewed by Brooks (2012) and commenced with the volumetrically minor Lower Basalts (~61–57 Ma, Hansen & Nielsen, 1999), which were followed by rapid eruption of >6 km of predominantly tholeiitic flood basalts (the Plateau Basalts) over a short period (55 ± 0.5 Ma) (Pedersen *et al.*, 1997; Larsen & Saunders, 1998; Storey *et al.*, 2007). This dramatic increase in magma productivity is probably associated with rapid decompression melting during the initial stages of continental break-up (Tegner *et al.*, 1998*a*; Storey *et al.*, 2007). The Plateau Basalt succession has been sampled extensively on a flow-by-flow basis (e.g. Larsen *et al.*, 1989) and therefore provides an excellent opportunity to investigate spatial, temporal and compositional variations during the generation of a flood basalt province associated with continental break-up.

The samples studied here are from the well-characterized Sortebræ profile in the Blosseville Coast region. The Plateau Basalt sequence here has been subdivided into four stratigraphic formations (from oldest to youngest, the Milne Land, Geikie Plateau, Rømer Fjord and Skrænterne Formations) on the basis of lithology, petrography, composition and photogrammetry (Larsen & Watt, 1985; Larsen *et al.*, 1989; Pedersen *et al.*, 1997) (Fig. 1). Two chemically distinct basalt suites have been identified and defined by Tegner *et al.* (1998*a*). The volumetrically dominant high-Ti suite with $TiO_2 = 1{\cdot}6$–$6{\cdot}2$ wt % and characteristically light rare earth element (LREE)-enriched compositions ($La/Sm_N = 1{\cdot}2$–$2{\cdot}1$) has been the focus of several detailed studies (Tegner *et al.*, 1998*a*; Andreasen *et al.*, 2004; Barker *et al.*, 2006; Peate *et al.*, 2008). The subordinate low-Ti suite (48 out of 391 flows, predominantly from the upper portion of the Milne Land Formation) with $TiO_2 = 0{\cdot}8$–$2{\cdot}0$ wt % and characteristic LREE-depleted compositions ($La/Sm_N = 0{\cdot}4$–$0{\cdot}9$) is the focus of this investigation. LREE-depleted and -enriched groupings are also recognized in the contemporaneous and conjugate Faroe Island (FI) lavas (Larsen *et al.*, 1999; Holm *et al.*, 2001; Søager & Holm, 2009, 2011).

Increasing La/Sm and decreasing Dy/Yb with stratigraphic height in the high-Ti lavas of the Milne Land and Geikie Plateau Formations were attributed to cooling of the plume source with decreasing depth of melting (Tegner *et al.*, 1998*a*). However, more recent studies have shown that these variations are also associated with changes in isotopic composition, indicating that mantle source variability also controlled the geochemical variations (Barker *et al.*, 2006). Source variations in the high-Ti CEG lavas have also been correlated with similar variations observed on modern Iceland and stratigraphic variations ascribed to the passage of a zoned plume (e.g. Tegner *et al.* 1998*b*; Barker *et al.*, 2006). The contemporaneous low-Ti CEG lavas received less attention in these previous studies. Distinct contrasts in isotopic composition were noted between the high- and low-Ti lavas, however, and were used to indicate the presence of a contemporaneous depleted mantle source during rift-related magmatism (Tegner *et al.*, 1998*a*), bearing some resemblance to that observed in the Northeastern Rift Zone on Iceland today (Barker *et al.*, 2006). More recently, the data presented here were used by Søager & Holm (2011) to compare low-Ti basaltic magmas on the Faroe Islands with those in CEG. Those workers suggested that the depleted magmas were derived from a regional depleted component termed the NAEM (the North Atlantic End-Member of Ellam & Stuart, 2000).

ANALYTICAL METHODS

The samples investigated here are mostly from the transition between the Milne Land and Geikie Plateau

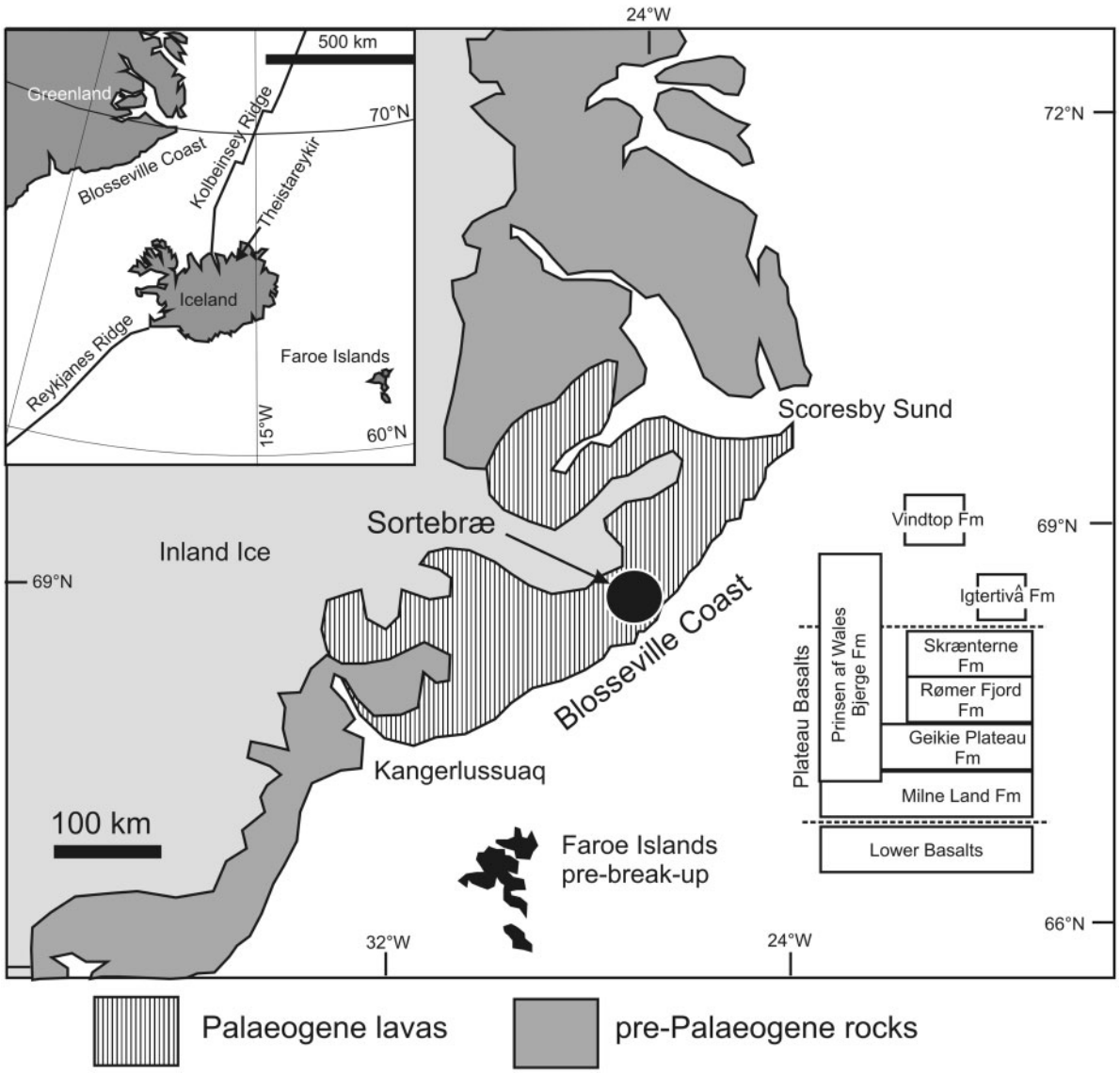

Fig. 1. Location map of the Central East Greenland (CEG) volcanism, showing the location of the Sorterbrae profile, and stratigraphic details [modified from Andreasen *et al.* (2004) and Peate *et al.* (2008)]. Also shown are the locations of potential correlatives to the CEG low-Ti magmas on Iceland and adjacent ridges and the Faroe Islands. The location of the Faroe Islands before continental break-up is indicated on the main map.

Formations, with additional low-Ti samples from the Rømer Fjord and Skrænterne Formations (see Fig. 1). The low-Ti basalts range from aphyric to sparsely porphyritic with plagioclase and olivine phenocrysts and minor clinopyroxene (Momme *et al.*, 2002; Andreasen *et al.*, 2004). A subset of high-Ti lavas was also analyzed to complement the isotopic datasets of Peate & Stecher (2003), Andreasen *et al.* (2004) and Barker *et al.* (2006). Weathered or altered surfaces and zeolite-filled vesicles were removed from samples before jaw-crushing and final powdering in a tungsten carbide ball mill. Major and trace element data for 15 low-Ti and five high-Ti samples are presented in Tables 1–3; major and trace element data for some of these and other Sortebrae profile samples have been discussed and/or presented previously by Tegner *et al.* (1998*a*), Momme *et al.* (2002, 2006) and Andreasen *et al.* (2004). Major elements (Table 1) were determined at the Geological Survey of Denmark and Greenland by X-ray fluorescence (XRF) using methods described by Kystol & Larsen (1999), who provided details on precision and reproducibility; major element data are typically precise to ±0·1 wt % (1 SD) or better. Loss on ignition (LOI) is relatively high in some samples; however, no correlations were observed between LOI and elemental concentrations,

Table 1: XRF major and trace element data

	Low-Ti																High-Ti				
Sample:	404230	83820	404232	404241	83834	83835	404266	404263	404262	404256	404250	404290	435634	83893	412493		83831	83857	83837	83838	83885
Flow no.:	63	64	65	72	77	78	79	81	82	88	94	142	180	194	253		70	76	80	80	182
Unit:	MLF	MLF	MLF	MLF	MLF	MLF	MLF	MLF	MLF	MLF	MLF	GPF	GPF	RFF	SKF		MLF	MLF	MLF	MLF	GPF
SiO_2	44·88	45·30	47·86	45·71	45·60	48·53	48·16	48·31	46·31	47·24	48·32	48·97	48·70	48·36	48·40		47·81	45·66	45·26	47·98	48·29
TiO_2	0·86	0·68	1·13	0·87	0·87	1·21	1·23	0·99	0·80	1·13	1·58	1·37	1·13	1·40	1·24		2·35	4·02	4·04	3·01	2·85
Al_2O_3	11·87	12·30	14·88	13·46	13·54	14·40	14·06	14·75	12·86	14·73	13·51	13·78	14·38	13·50	14·15		13·36	12·67	12·42	13·36	13·61
Fe_2O_3	3·17	4·81	2·84	3·33	4·07	5·82	3·33	3·91	2·46	4·27	6·18	4·07	4·57	3·63	5·62		6·13	8·11	7·02	5·72	4·89
FeO	7·89	5·29	8·19	7·54	6·58	6·24	8·30	6·21	7·79	7·05	8·24	8·71	7·55	8·80	6·67		7·46	7·73	8·84	8·68	8·61
MnO	0·18	0·17	0·18	0·18	0·17	0·20	0·20	0·18	0·18	0·18	0·25	0·22	0·21	0·23	0·20		0·21	0·24	0·26	0·22	0·23
MgO	15·29	16·60	8·42	13·56	12·80	7·48	8·26	9·17	14·26	7·43	6·86	7·17	7·95	7·44	7·50		6·62	5·91	5·59	5·98	6·03
CaO	10·02	10·21	12·77	10·80	10·83	11·58	12·30	12·84	10·92	12·91	11·49	12·30	12·33	11·41	11·98		11·47	8·80	10·37	10·37	11·09
Na_2O	1·06	1·12	1·88	1·32	1·27	2·82	1·91	1·78	1·33	1·81	2·21	2·09	1·94	2·40	2·19		2·15	2·86	2·46	2·56	2·14
K_2O	0·04	0·04	0·09	0·03	0·01	0·11	0·07	0·05	0·04	0·05	0·11	0·09	0·06	0·16	0·09		0·14	0·71	0·16	0·12	0·12
P_2O_5	0·07	0·07	0·10	0·07	0·07	0·12	0·11	0·09	0·07	0·10	0·16	0·12	0·10	0·12	0·11		0·24	0·43	0·44	0·32	0·31
LOI	4·39	4·48	1·54	2·90	4·09	1·99	1·71	1·39	2·79	2·83	1·65	0·83	1·35	1·94	1·81		2·16	3·25	3·28	2·37	2·22
Total	99·72	101·07	99·89	99·76	99·90	100·50	99·64	99·67	99·80	99·72	100·56	99·71	100·27	99·37	99·95		100·10	100·39	100·14	100·69	100·39
Nb	1·1	0·9	0·8	1·8	0·7	1·8	1·2	0·9	0·7	1·2	1·6	1·6	2·4	2·6	3·8		15·8	16·5	26·4	26·0	12·5
Zr	44·1	43·5	43·5	56·6	34·5	68·6	54·2	40·3	46·7	58·9	69·7	54·6	73·8	88·3	67·7		193·2	204·4	284·0	279·9	149·1
Y	18·7	20·8	21·1	26·4	18·5	32·2	26·4	21·0	25·8	30·5	33·7	29·4	34·1	39·3	28·3		36·5	39·0	47·9	47·4	33·3
Sr	92·8	79·5	80·3	102·6	51·8	99·4	219·3	79·8	76·6	88·3	103·3	73·6	87·2	95·8	123·8		243·6	252·1	235·6	230·8	212·2
Rb	1·0	1·3	0·3	1·0	1·3	1·5	0·7	0·6	0·9	0·9	3·4	0·7	1·0	1·3	0·5		0·9	1·4	1·5	16·9	0·7
La	2·3	2·4	1·4	2·2	2·8	3·9	1·8	2·1	1·1	1·2	1·1	2·7	2·5	4·1	3·4		12·5	11·7	18·3	18·4	10·6
Ce	6·3	6·4	5·1	4·7	2·5	9·6	4·7	3·3	4·2	3·1	3·6	3·7	8·4	9·7	9·7		35·8	36·6	53·9	54·1	29·6
Nd	5·2	5·2	4·9	5·1	3·8	7·1	5·8	5·6	4·7	5·6	4·2	5·4	7·1	8·4	6·9		25·0	27·7	35·7	37·0	21·8
Zn	79·5	70·6	65·7	74·1	70·9	91·6	75·5	70·0	75·5	82·2	92·4	88·3	96·1	96·8	78·9		106·2	109·4	139·0	144·3	93·9
Cu	86·6	114·9	86·7	124·9	86·8	153·1	114·5	113·4	96·2	132·8	152·2	130·0	159·4	226·0	124·1		182·5	142·8	208·5	97·8	192·7
Ni	548·0	398·5	446·4	124·4	734·6	116·3	124·5	538·4	163·2	135·1	94·1	116·4	79·8	66·7	96·1		74·6	77·4	80·4	76·2	79·5
Cr	913·8	738·6	929·2	352·0	1111·0	264·2	339·9	864·0	368·7	297·4	232·9	295·1	103·2	75·0	164·3		66·2	103·7	52·3	47·6	126·6
V	203·8	233·5	234·9	316·0	205·8	343·8	290·7	245·6	304·1	343·9	378·9	329·7	366·7	367·4	311·6		398·4	397·3	521·0	504·3	332·3
Ba	13·8	14·5	21·7	20·1	12·3	31·9	25·6	19·2	13·0	23·7	600·3	23·8	25·7	29·7	39·0		76·6	80·7	129·2	143·4	71·9
Sc	29·4	34·2	34·1	43·9	30·6	47·6	40·6	37·0	45·8	43·0	49·0	43·1	46·1	51·1	43·3		35·9	39·6	38·3	41·8	36·7

Major elements determined at the Geological Survey of Denmark and Greenland using methods described by Kystol & Larsen (1999). Trace elements determined at the University of Edinburgh using methods described by Fitton *et al.* (1998). MLF, Milne Land Formation; GPF, Geikie Plateau Formation; RFF, Rømer Fjord Formation; SKF, Skrænterne Formation.

ratios or isotopic compositions, which might indicate that alteration has influenced the dataset. Some trace elements were determined on pressed powder pellets by XRF at the University of Edinburgh (Table 1) using methods and reproducibilities described by Fitton *et al.* (1998).

Original inductively coupled plasma mass spectrometry (ICP-MS) trace element data for Th, U and Pb in the Sortebræ profile (as discussed by Tegner *et al.*, 1998*a*; Momme *et al.*, 2002, 2006; Barker, 2006; Barker *et al.*, 2006; Peate *et al.*, 2008) were found to be inaccurate on the basis of large degrees of scatter on mantle-normalized multi-element diagrams. The samples were therefore reanalysed by ICP-MS at the Victoria University of Wellington using methods described by McCoy-West *et al.* (2010) (Table 2) and the new data produce much smoother and more realistic variations. Details of the reproducibility and accuracy of the method, based on duplicate analyses of standards, are presented in Supplementary Data Appendix A (available for downloading at http://www.petrology.oxfordjournals.org). In brief, most trace elements of relevance to this study show good agreement with reference values and reproducibilities better than

Table 2: ICP-MS trace element data

	Low-Ti															High-Ti				
Sample:	404230	83820	404232	404241	83834	83835	404266	404263	404262	404256	404250	404290	435634	83893	412493	83831	83857	83837	83838	83885
Flow no.:	63	64	65	72	77	78	79	81	82	88	94	142	180	194	253	70	76	80	80	182
Unit:	MLF	MLF	MLF	MLF	MLF	MLF	MLF	MLF	MLF	MLF	MLF	GPF	GPF	RFF	SKF	MLF	MLF	MLF	MLF	GPF
Li	7·13	8·61	6·97	10·25	8·64	5·76	5·03	4·91	6·07	6·20	13·89	9·65	5·93	6·92	7·48	5·78	6·36	6·92	8·35	4·18
Sc	38·47	42·47	43·13	50·08	37·69	50·94	50·90	41·72	52·25	50·72	51·54	50·96	53·02	51·97	50·30	37·03	39·03	39·82	39·46	42·01
Ti	0·93	0·89	0·90	1·18	0·70	1·27	1·14	0·83	1·03	1·26	1·43	1·17	1·38	1·69	1·30	2·98	3·10	4·30	4·22	2·45
V	255·52	270·91	266·81	334·82	232·51	355·92	334·59	266·10	330·88	372·53	403·86	361·77	401·70	452·23	357·90	415·21	433·49	543·26	524·79	400·46
Cr	970·17	763·80	945·57	390·37	1148·55	255·86	377·35	880·34	400·92	316·28	241·00	327·00	115·49	81·20	193·38	61·55	100·11	46·68	43·43	136·78
Co	77·50	67·25	72·42	53·46	72·24	51·97	55·18	68·63	51·99	54·73	53·97	52·72	56·54	57·33	54·91	50·38	52·28	52·93	52·83	54·86
Ni	528·89	368·84	454·92	135·74	663·53	112·24	129·25	542·91	177·08	148·14	99·87	121·02	83·42	70·60	98·30	69·68	74·97	76·24	71·00	83·04
Cu	111·07	128·79	131·67	162·03	120·02	223·12	168·11	147·28	160·70	177·31	226·10	188·09	183·47	270·48	148·93	240·19	231·01	312·69	146·53	245·79
Zn	75·91	67·61	74·08	80·04	67·64	90·45	84·92	77·21	78·04	91·18	100·77	98·26	101·93	117·25	93·69	114·92	124·74	155·43	153·17	111·12
Ga	13·96	14·60	15·28	18·37	12·89	18·29	20·65	15·00	18·12	19·29	18·59	18·94	18·91	20·03	18·69	23·99	25·03	27·60	26·76	22·23
Rb	0·81	1·11	0·48	1·01	1·22	1·47	0·54	0·70	0·75	1·03	3·26	0·77	0·87	1·23	0·50	0·31	0·98	1·24	16·96	0·46
Sr	99·56	80·63	85·16	106·95	54·66	102·63	224·85	84·99	79·82	91·23	105·12	74·89	87·71	98·03	129·03	243·53	251·75	241·87	234·13	211·24
Y	19·84	20·56	21·50	25·84	18·20	31·75	26·00	21·05	25·50	30·27	32·94	28·91	32·52	37·29	27·64	33·94	37·23	46·77	46·77	31·64
Zr	49·41	41·44	44·95	58·65	35·49	69·56	56·15	41·55	49·06	59·43	72·02	53·21	75·39	88·36	69·32	195·63	207·13	287·40	285·85	150·98
Zr	49·27	41·52	45·06	58·23	35·03	69·61	56·30	41·78	48·52	59·60	71·56	53·60	73·70	86·78	69·28	190·12	205·97	291·30	289·21	150·49
Nb	1·22	0·98	1·09	1·90	0·67	1·88	1·40	0·92	0·95	1·34	1·83	0·83	2·46	3·05	4·07	15·32	15·94	25·63	25·23	8·58
Cs	0·13	0·26	0·06	0·02	0·15	0·01	0·04	0·02	0·01	0·02	0·22	0·01	0·01	0·01	0·00	0·01	0·01	0·02	0·06	0·00
Ba	13·43	10·37	17·21	19·67	9·13	27·11	18·52	16·08	9·66	14·94	587·52	19·73	20·19	24·83	32·68	54·46	58·59	93·27	114·85	54·11
La	1·76	1·45	1·59	2·16	1·01	2·98	1·82	1·16	1·26	1·61	2·14	1·55	2·83	3·40	3·83	13·82	14·45	21·81	21·56	10·80
Ce	5·16	4·45	4·78	6·34	11·91	8·31	5·52	3·75	4·07	5·27	6·41	4·92	7·80	9·41	9·81	35·48	37·70	55·92	56·03	28·30
Pr	0·90	0·81	0·86	1·11	0·59	1·35	1·01	0·71	0·80	1·00	1·18	0·90	1·32	1·64	1·53	5·32	5·63	8·16	8·09	4·17
Nd	5·23	4·74	5·01	6·31	3·53	7·47	5·82	4·16	4·92	5·97	6·89	5·38	7·39	8·95	8·01	25·26	26·70	37·06	37·36	19·50
Sm	2·02	1·92	1·99	2·52	1·53	2·89	2·40	1·79	2·09	2·51	2·93	2·28	2·85	3·44	2·79	6·67	7·04	9·61	9·47	5·26
Eu	0·80	0·78	0·81	1·01	0·64	1·12	0·96	0·74	0·86	1·01	1·29	0·92	1·11	1·29	1·09	2·20	2·34	3·08	3·07	1·81
Gd	2·76	2·60	2·71	3·55	2·20	3·97	3·41	2·52	3·05	3·64	4·23	3·32	3·90	4·75	3·78	6·98	7·64	10·17	10·04	5·87
Tb	0·50	0·51	0·53	0·65	0·43	0·77	0·65	0·50	0·60	0·71	0·80	0·65	0·77	0·88	0·68	1·10	1·19	1·53	1·53	0·95
Dy	3·49	3·58	3·70	4·54	3·09	5·43	4·53	3·56	4·20	5·04	5·69	4·73	5·47	6·37	4·73	6·67	7·24	9·02	9·01	5·89
Ho	0·74	0·75	0·80	0·95	0·66	1·17	0·98	0·78	0·93	1·09	1·21	1·04	1·18	1·37	1·03	1·29	1·40	1·75	1·74	1·16
Er	2·05	2·12	2·27	2·70	1·92	3·35	2·80	2·24	2·72	3·22	3·51	3·08	3·43	3·97	2·94	3·44	3·76	4·64	4·63	3·26
Tm	0·29	0·31	0·34	0·39	0·29	0·49	0·41	0·33	0·40	0·47	0·51	0·45	0·51	0·58	0·43	0·47	0·51	0·62	0·64	0·44
Yb	1·87	1·98	2·13	2·50	1·83	3·17	2·65	2·12	2·56	3·07	3·31	3·06	3·32	3·78	2·81	2·90	3·16	3·84	3·90	2·79
Lu	0·27	0·30	0·31	0·37	0·27	0·46	0·39	0·31	0·38	0·46	0·48	0·45	0·49	0·56	0·41	0·40	0·45	0·53	0·55	0·40
Hf	1·43	1·21	1·34	1·65	1·06	2·06	1·63	1·24	1·49	1·71	2·08	1·52	2·14	2·37	1·92	4·85	5·28	7·28	7·25	3·77
Ta	0·15	0·58	0·11	0·22	0·07	0·19	0·18	0·45	0·13	0·16	0·33	0·13	0·41	0·24	0·37	0·99	1·07	1·66	1·66	0·51
W	5·51	14·15	4·91	16·40	7·91	15·42	12·14	11·87	13·45	23·97	20·12	0·36	28·14	23·49	7·71	13·03	14·13	7·90	6·31	15·97
Pb	0·49	0·43	0·37	0·44	0·23	0·76	0·40	0·28	0·28	0·33	0·49	0·31	0·47	0·58	0·88	1·44	1·51	2·07	2·13	1·18
Th	0·23	0·11	0·16	0·17	0·07	0·37	0·22	0·09	0·10	0·13	0·39	0·13	0·26	0·30	0·44	1·08	1·14	1·80	1·83	0·85
U	0·05	0·03	0·04	0·05	0·02	0·09	0·04	0·02	0·03	0·03	0·05	0·03	0·07	0·08	0·12	0·32	0·33	0·52	0·54	0·26

ICP-MS trace element data determined at Victoria University of Wellington using methods described by McCoy-West *et al*. (2010). Details on reproducibility and accuracy based on replicate analyses of standards are given in Supplementary Data Appendix A.

Table 3: REE-ID data

	Low-Ti															High-Ti				
Sample:	404230	83820	404232	404241	83834	83835	404266	404263	404262	404256	404250	404290	435634	83893	412493	83831	83857	83837	83838	83885
Flow no.	63	64	65	72	77	78	79	81	82	88	94	142	180	194	253	70	76	80	80	182
Unit	MLF	MLF	MLF	MLF	MLF	MLF	MLF	MLF	MLF	MLF	MLF	GPF	GPF	RFF	SKF	MLF	MLF	MLF	MLF	GPF
La	1·60	–	1·48	2·05	0·97	2·71	1·75	1·05	1·17	1·54	2·17	1·51	2·81	3·20	3·62	13·41	13·97	20·90	20·33	10·37
Ce	4·74	–	4·50	6·07	3·09	7·55	6·31	3·44	3·85	5·66	6·29	4·66	7·82	9·40	9·24	36·10	36·93	54·32	52·58	26·96
Nd	4·76	–	4·61	6·13	3·45	6·81	5·52	3·91	4·53	5·66	6·69	5·07	7·35	8·63	7·53	24·58	25·80	35·95	35·27	18·75
Sm	1·84	–	1·84	2·42	1·46	2·62	2·23	1·64	1·95	2·38	2·77	2·11	2·80	3·25	2·60	6·46	6·80	9·14	8·98	5·06
Eu	0·73	–	0·75	0·98	0·61	1·02	0·90	0·68	0·81	0·97	1·10	0·86	1·08	1·23	1·02	2·16	2·26	2·93	2·88	1·70
Gd	2·65	–	2·77	3·59	2·34	3·87	3·37	2·66	3·13	4·02	4·51	3·35	4·60	4·89	3·62	7·21	7·46	9·84	9·41	5·66
Dy	3·16	–	3·44	4·26	2·94	4·94	4·32	3·33	4·01	4·83	5·46	4·49	5·43	5·99	4·49	6·59	7·03	8·79	8·89	5·64
Er	1·92	–	2·16	2·62	1·88	3·12	2·70	2·15	2·60	3·10	3·68	2·99	3·67	3·86	2·84	3·42	3·67	4·51	4·44	3·08
Yb	1·71	–	1·94	2·33	1·73	2·85	2·45	1·99	2·41	2·87	3·11	2·83	3·23	3·59	2·63	2·81	3·03	3·66	3·60	2·62
Lu	0·25	–	0·28	0·34	0·25	0·41	0·36	0·29	0·35	0·42	0·45	0·42	0·47	0·53	0·38	0·40	0·43	0·51	0·50	0·37

Rare earth elements determined by isotope dilution MC-ICP-MS using methods described in detail by Baker *et al.* (2002); –, not analysed.

3% (2 SD), with the exception of Th (5%), Nb (6%) and Pb (12%). REE concentrations were determined by multi-collector (MC)-ICP-MS isotope dilution (REE-ID) using the methods described in detail by Baker *et al.* (2002) (Table 3). REE-ID concentrations are considered to be reproducible to better than 1% and REE ratios to 0·2% (2 SD). Comparison of the original ICP-MS REE dataset discussed by Tegner *et al.* (1998*a*) and both the new isotope dilution data and ICP-MS data presented here indicates a tendency to higher middle REE (MREE) in our new dataset (i.e. higher Dy and thus higher Dy/Yb). All the trace element diagrams presented below are constructed using our new ICP-MS and REE-ID data unless stated otherwise.

All the isotope data presented here are new and were measured by MC-ICP-MS on an Axiom system at the Danish Lithosphere Centre, Copenhagen, and are presented in Table 4. Sr isotopes were determined on ~1 g of whole-rock powder leached in hot 6 N HCl for 3 h then washed several times with MQ water to remove secondary and/or weathered material, and then dissolved using HF–HNO_3–HCl. Sr cuts were then analyzed using methods described in detail by Waight *et al.* (2002). Nd isotopes were determined on unleached aliquots of the same powder and were dissolved using the same methods. The samples were passed through conventional cation exchange columns to yield a bulk REE cut. An additional Ba clean-up step was carried out using RE-spec resin and the solutions were analyzed by MC-ICP-MS using methods similar to those of Luais *et al.* (1997). Hf isotopes were determined by MC-ICP-MS on ~100 mg of powder dissolved using flux fusion techniques and analysed using protocols described by Ulfbeck *et al.* (2003). Most Pb analyses were performed on hand-picked chips leached for 3 h in cold 6 N HCl to exclude possible contamination during crushing and to remove secondary and/or weathered material. Rocks chips were not available for several samples (83893, 83835, 83837 and 83831) and Pb isotope compositions for these were determined on whole-rock powders leached in hot 6 N HCl for 3 h. Pb isotopes were determined using a ^{207}Pb–^{204}Pb double spike following methods given by Baker *et al.* (2004).

To compare more accurately Eocene CEG and Icelandic basalt compositions, it is necessary to take into account the evolution of the mantle source since 55 Ma. No source or age correction is applied to the Sr isotope data as Rb/Sr ratios in unleached powders are low (<0·03), resulting in relatively small corrections for ingrowth over 55 Myr. Leaching of powders prior to analysis also preferentially removes ingrown radiogenic Sr to yield initial Sr isotopic compositions (e.g. Thirlwall *et al.*, 1994). Source-corrected Hf and Nd isotopic compositions ($\varepsilon_{Nd(sc)}$ and $\varepsilon_{Hf(sc)}$) are calculated by age-correcting the data to 55 Ma using measured Sm–Nd (REE-ID) and Lu–Hf (ICP-MS) ratios ($\varepsilon_{Nd(i)}$ and $\varepsilon_{Hf(i)}$). The appropriate parent/daughter ratio needed to derive this initial composition from a 2 Ga Bulk Earth source is calculated and used to forward-correct to a present-day source-corrected composition (Salters & White, 1998; see also Barker *et al.*, 2006). Sm/Nd in the low-Ti lavas is

Table 4: Sr–Nd–Hf–Pb isotope data

Sample	Flow no.	$^{87}Sr/^{86}Sr$ meas.	$^{147}Sm/^{144}Nd$	$^{143}Nd/^{144}Nd$ meas.	εNd (i)	εNd (sc)	$^{177}Lu/^{176}Hf$	$^{177}Hf/^{176}Hf$ meas.	εHf (i)	εHf (sc)	$^{206}Pb/^{204}Pb$ meas.	$^{207}Pb/^{204}Pb$ meas.	$^{208}Pb/^{204}Pb$ meas.
Low-Ti													
412493	253	0·703273 ± 13	0·2061	0·513013 ± 7	7·25	7·47	0·0317	0·283186 ± 5	14·70	15·10	18·0608	15·4189	38·1302
412493 (dup)							0·0317	0·283184 ± 6	14·64	15·04			
83893	194	0·702931 ± 15	0·2244	0·513041 ± 9	7·67	7·89	0·0362	0·283161 ± 6	13·65	14·02	18·0084	15·4092	37·9095
435634	180	0·702962 ± 21	0·2269	0·513035 ± 7	7·52	7·74	0·0358	0·283163 ± 5	13·76	14·13	18·0734	15·4104	37·9810
404290	142	0·702912 ± 17	0·2486	0·513074 ± 6	8·15	8·39	0·0440	0·283190 ± 6	14·39	14·78	18·3238	15·4289	38·0370
404250	94	0·702981 ± 15	0·2471	0·513042 ± 6	7·52	7·74	0·0343	0·283155 ± 6	13·53	13·89	17·8971	15·3786	37·9622
404256	88	0·702871 ± 14	0·2498	0·513101 ± 6	8·66	8·91	0·0387	0·283217 ± 6	15·53	15·95	17·8946	15·3847	37·7370
404262	82	0·702743 ± 17	0·2558	0·513154 ± 6	9·66	9·93	0·0400	0·283241 ± 5	16·36	16·80	17·8368	15·3706	37·6371
404263	81	0·702734 ± 15	0·2507	0·513148 ± 7	9·56	9·84	0·0384	0·283247 ± 7	16·62	17·07	17·7448	15·3665	37·6367
404266	79	0·703008 ± 15	0·2403	0·513092 ± 6	8·55	8·80	0·0361	0·283192 ± 10	14·74	15·14	17·7365	15·3662	37·8063
404266 (dup)							0·0361	0·283195 ± 4	14·86	15·26			
83835	78	0·703658 ± 15	0·2291	0·512960 ± 6	6·05	6·23	0·0337	0·283173 ± 4	14·19	14·57	17·6212	15·3824	38·1225
83835 (dup)							0·0337	0·283166 ± 6	13·92	14·30			
83834	77	0·702655 ± 15	0·2520	0·513166 ± 7	9·91	10·20	0·0373	0·283278 ± 7	17·75	18·23	17·7300	15·3594	37·5935
404241	72	0·702738 ± 18	0·2349	0·513156 ± 7	9·83	10·10	0·0291	0·283277 ± 6	18·03	18·52	18·1341	15·4377	38·0207
404232	65	0·702930 ± 17	0·2376	0·513101 ± 8	8·74	8·99	0·0357	0·283228 ± 7	16·04	16·48	17·6901	15·3734	37·9414
83820	64	0·702833 ± 15	0·2234	0·513138 ± 8	9·57	9·84	0·0344	0·283259 ± 7	17·20	17·67	17·8372	15·3969	37·8584
404230	63	0·702981 ± 15	0·2300	0·513073 ± 7	8·25	8·49	0·0296	0·283218 ± 9	15·93	16·36	17·5890	15·3562	38·0285
High-Ti													
83885	182	0·703177 ± 11	0·1608	0·512962 ± 6	6·58	6·77	0·0154	0·283068 ± 6	11·16	11·46	18·3280	15·4255	38·1656
83838	80	0·703328 ± 13	0·1517	0·512972 ± 8	6·83	7·03	0·0112	0·283062 ± 6	11·09	11·39	18·5165	15·4576	38·3654
83838 (dup)											18·5166	15·4580	38·3675
83837	80	0·703189 ± 13	0·1514	0·512976 ± 8	6·91	7·11	0·0111	0·283066 ± 6	11·23	11·53	18·4267	15·4386	38·2643
83857	76	0·703153 ± 13	0·1570	0·512981 ± 7	6·98	7·18	0·0132	0·283095 ± 7	12·17	12·50	18·3098	15·4367	38·2024
83831	70	0·703175 ± 13	0·1565	0·512988 ± 8	7·11	7·32	0·0119	0·283090 ± 6	12·05	12·38	18·2735	15·4273	38·1903

Age-corrected values are calculated using ICP-MS or REE-ID data. Over the period of analysis, replicate analyses of standards were as follows: SRM987 ($n = 19$) $^{87}Sr/^{86}Sr = 0·710254 \pm 24$ (2 SD); DLC in-house mixed Ames Nd–Sm metal ($n = 13$) $^{143}Nd/^{144}Nd = 0·512126 \pm 13$ (2 SD) (equivalent to $^{143}Nd/^{144}Nd = 0·511860$ for La Jolla Nd); DLC in-house Hf standard ($n = 11$) $^{177}Hf/^{176}Hf = 0·281876 \pm 16$ (2 SD) equivalent to a value of $^{177}Hf/^{176}Hf = 0·28216$ for the JMC475 standard; SRM981 ($n = 5$) $^{206}Pb/^{204}Pb = 16·941 \pm 1$, $^{207}Pb/^{204}Pb = 15·499 \pm 1$ and $^{208}Pb/^{204}Pb = 36·721 \pm 2$ (2 SD). ε_{Nd} and ε_{Hf} are calculated using values for CHUR of $^{147}Sm/^{144}Nd = 0·1966$, $^{143}Nd/^{144}Nd = 0·512638$, $^{176}Lu/^{177}Hf = 0·0332$ and $^{177}Hf/^{176}Hf = 0·282772$.

similar to that of the depleted mantle, so this results in minor differences between $\varepsilon_{Nd(sc)}$ and $\varepsilon_{Nd(0)}$ (±0·1 ε units). The lower Sm/Nd of the high-Ti lavas results in a difference of *c.* 0·5 ε units between $\varepsilon_{Nd(sc)}$ and $\varepsilon_{Nd(0)}$. Similarly, $\varepsilon_{Hf(sc)}$ is ∼0·1–0·6 (average = 0·4) ε units higher than $\varepsilon_{Hf(0)}$ for the low-Ti basalts and ∼1 ε unit higher in the high-Ti basalts.

Pb isotopes are presented using measured values with vectors on relevant diagrams indicating the maximum and minimum age correction applicable. Age correction of the low-Ti basalt Pb isotope data to 55 Ma using ICP-MS U–Th–Pb concentrations results in decreases in $^{206}Pb/^{204}Pb$, $^{207}Pb/^{204}Pb$ and $^{208}Pb/^{204}Pb$ of 0·04–0·08, 0·002–0·004 and 0·04–0·14 for the low-Ti basalts and 0·12–0·14, 0·006 and 0·13–0·15 for the high-Ti basalts, respectively. As U/Pb and Th/Pb ratios increase in lavas relative to their mantle sources during partial melting, present-day mantle source compositions will be similar to, or slightly less radiogenic than the measured present-day compositions of the lavas.

RESULTS

Major and trace elements

The low-Ti basalts are tholeiitic, with five samples classifying as picrites (MgO > 12%) following Le Bas (2000). They are distinguished from the high-Ti basalts by generally higher MgO, Ni and Cr contents and lower TiO_2, $FeO_{(tot)}$, K_2O, Na_2O, P_2O_5, Nb, Zr, Sr, LREE and Ba (Fig. 2; see also Tables 1 and 3). Excluding the high-MgO samples (assumed to have accumulated olivine; Momme *et al.*, 2002), trends of increasing incompatible elements and decreasing CaO, Al_2O_3, Ni and Cr with decreasing MgO are similar to those observed in the high-Ti basalts and suggest fractionation of olivine, clinopyroxene and plagioclase (Andreasen *et al.*, 2004). Increasing FeO_{tot}, P_2O_5 and TiO_2 with decreasing MgO indicate that Fe–Ti oxides and apatite were not important fractionating phases. The CEG low-Ti and Faroe Island (FI) low-Ti basalts have similar compositions, although the latter tend to have somewhat higher and more scattered K_2O and Rb contents (Fig. 2), possibly as a result of varying degrees of alteration.

The low-Ti basalts analyzed in this study have $La_N/Sm_N = 0{\cdot}37–0{\cdot}62$, with two possibly crustally contaminated samples (based on their higher $^{87}Sr/^{86}Sr$) having slightly higher values (samples 83835 and 412493 with $La_N/Sm_N = 0{\cdot}639$ and $0{\cdot}858$ respectively) (Fig. 3, Table 3). The heavy REE (HREE) patterns are typically flat to slightly HREE depleted ($Dy_N/Yb_N = 1{\cdot}03–1{\cdot}25$). The low-Ti basalts are characterized by small and generally negative Eu anomalies ($Eu/Eu^* = 0{\cdot}92–1{\cdot}01$). These compositions contrast markedly with the high-Ti lavas with $La_N/Sm_N = 1{\cdot}26–1{\cdot}41$ and $Dy_N/Yb_N = 1{\cdot}38–1{\cdot}59$. REE concentrations (e.g. La) increase broadly with decreasing MgO (Fig. 2), consistent with olivine fractionation, but this has no significant effect on REE ratios such as La/Yb_N and Dy/Yb_N.

Primitive mantle-normalized multi-element patterns (Fig. 4) for the low-Ti basalts are relatively flat, MORB-like patterns with lower concentrations of most incompatible trace elements compared with the high-Ti basalts. Enrichment in Ba, K and Rb in a single sample (404250; Fig. 4, Table 1) is not an analytical artefact, as consistent results are observed for XRF and two independent ICP-MS analyses; the enrichment is possibly a consequence of alteration associated with zeolite-facies burial metamorphism and incomplete removal of secondary minerals during sample processing (Larsen *et al.*, 1989; Neuhoff *et al.*, 1997). The low-Ti basalts have trace element concentrations largely intermediate between an average Theistareykir composition and depleted Atlantic MORB, with a similar characteristic depletion in Pb. The low-Ti basalts display enrichment in Ba, similar to Theistareykir, but do not display the additional enrichments in Sr and Nb (Ta) considered characteristic of Icelandic depleted compositions (e.g. Stracke *et al.*, 2003).

A more detailed comparison of the incompatible trace element compositions of the CEG low-Ti basalts, MORB and depleted Icelandic compositions is possible using a MORB-normalized diagram (Fig. 5). Compared with global normal (N)-MORB the CEG low-Ti basalts have similar to generally lower concentrations of all incompatible trace elements. They are distinguished from N-MORB by having generally positive Sr peaks with Sr/Sr^* [$= Sr_{MN}/\sqrt{(Nd_{MN}*Zr_{MN})}$ where MN designates MORB normalized] between 0·8 and 2·8 (average = 1·3) and positive Pb peaks with Pb/Pb^* [$= Pb_{MN}/\sqrt{(La_{MN}*Nd_{MN})}$] of 1·1–1·8 (average = 1·4). The CEG low-Ti basalts are also generally relatively more depleted in LREE and Nb compared with MREE, HREE, Rb, Ba, Th and U than MORB, and exhibit a positive peak at Ba. Many of these features of the CEG low-Ti basalts are also shared with depleted Icelandic compositions such as Theistareykir; for example, the characteristic positive Sr and Ba peaks (Fig. 5). However, the CEG low-Ti basalts appear to be distinct from Theistareykir owing to the positive Pb peak (Theistareykir $Pb/Pb^* = 0{\cdot}6–0{\cdot}9$, average = 0·77), lower Nb and higher Zr, Hf, Th and U. We have also plotted the single full trace element analysis for an FI low-Ti basalt from Søager & Holm (2011) (sample 121516) in Fig. 5, and note that this is virtually identical to the CEG low-Ti basalts, showing similar distinctions from MORB and Theistareykir.

It is possible that the Pb enrichment seen in the CEG low-Ti lavas is a result of contamination during milling in a WC ball-mill (e.g. Chauvel & Hémond, 2000) or an analytical artefact. However, the presence of a positive Pb peak in both the FI and CEG samples suggests otherwise, as the FI sample was processed in agate (N. Søager, personal communication) and analysed independently at a separate laboratory (Søager & Holm, 2011). Furthermore, no consistent offsets are observed between $^{206}Pb/^{204}Pb$ determined on leached chips in this study, or on leached powders of the same samples published by Peate & Stecher (2003).

Isotopic data

The low-Ti basalts are distinct from other CEG magmatic suites with lower $^{87}Sr/^{86}Sr$ and higher $\varepsilon_{Nd(i)}$ (Fig. 6). They have $^{87}Sr/^{86}Sr$ ranging from 0·70266 to 0·70301, excluding two samples with higher $^{87}Sr/^{86}Sr$ up to 0·70366. Nd isotopic compositions at 55 Ma range from $\varepsilon_{Nd(i)}$ of +7·5 to +9·9; the two radiogenic $^{87}Sr/^{86}Sr$ samples have $\varepsilon_{Nd(i)} = +6{\cdot}1$ and +7·3. Hf isotopic compositions of the low-Ti basalts range from $\varepsilon_{Hf(i)}$ of +13·1 to +18·0. The low-Ti basalts have more radiogenic $\varepsilon_{Hf(i)}$ than contemporaneous Milne Land and Geikie Plateau Formation high-Ti basalts, and overlap with, and extend to more radiogenic values than, the overlying Rømer Fjord and Skrænterne Formation lavas (Fig. 6). The Pb isotope compositions of the low-Ti basalts fall within the range of

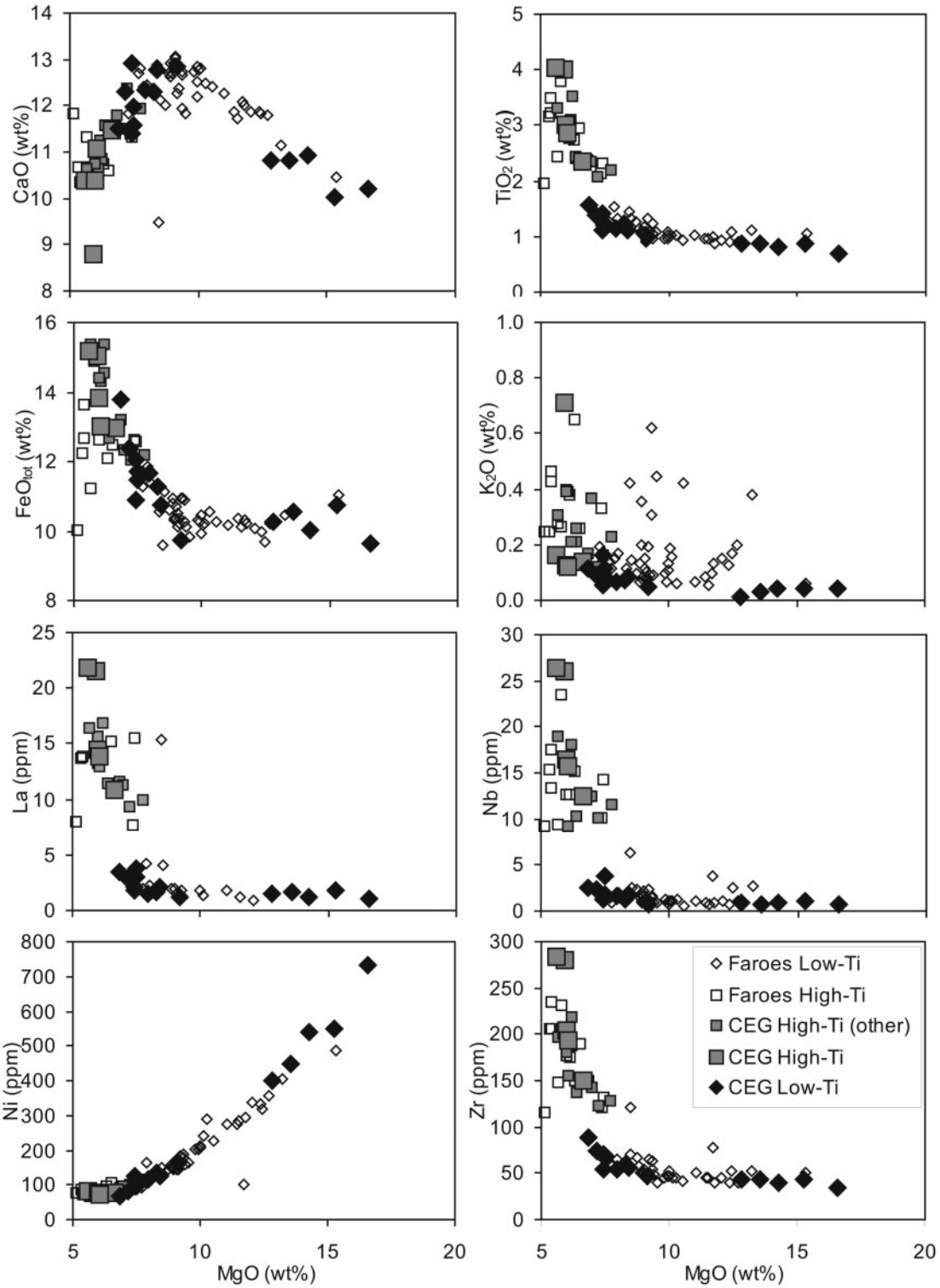

Fig. 2. Selected major and trace element variations for CEG basalts from this study versus MgO; additional CEG high-Ti data (labelled other) are from Andreasen *et al.* (2004). Data for the Faroe Islands basalts are plotted for comparison (Søager & Holm, 2009, 2011).

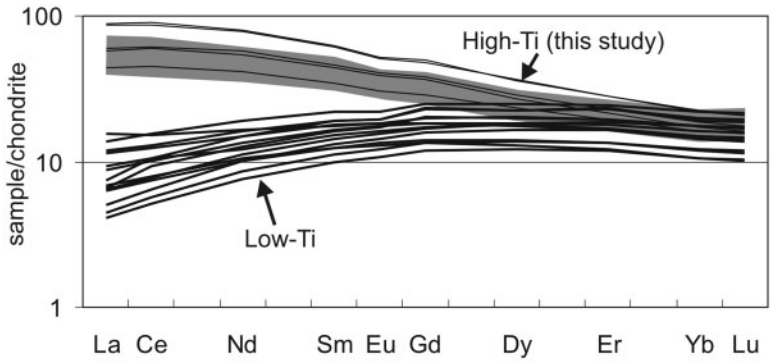

Fig. 3. Chondrite-normalized REE patterns for the high-Ti and low-Ti basalts; grey field represents high-Ti data from Andreasen *et al.* (2004); normalizing values from Anders & Grevesse (1989).

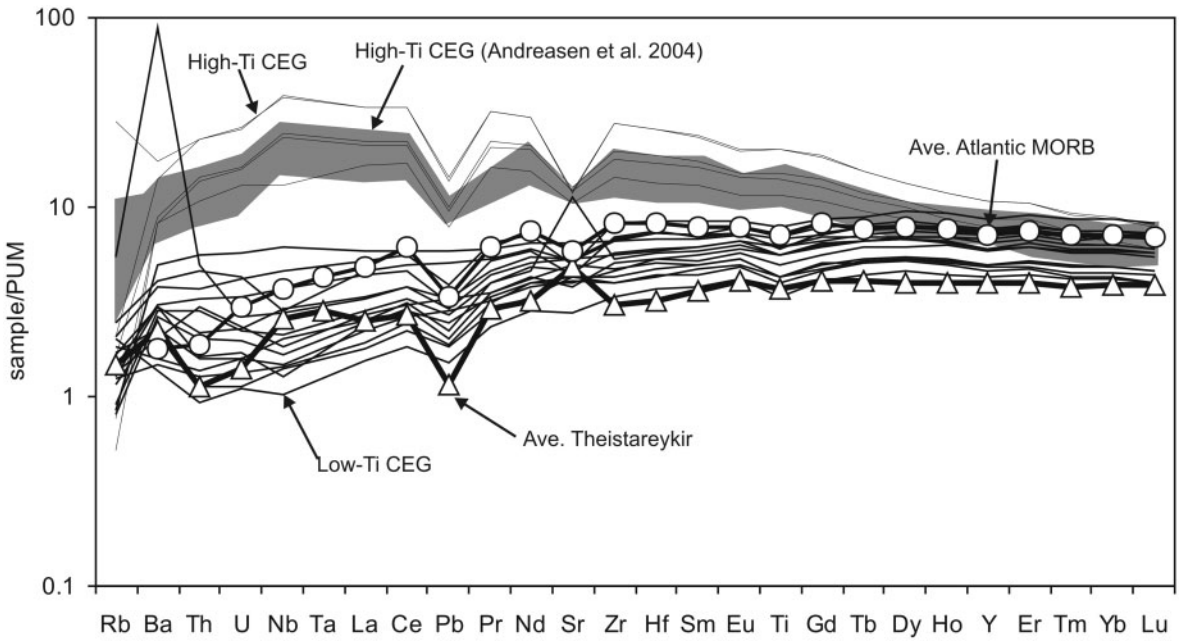

Fig. 4. Primitive upper mantle (PUM)-normalized multi-element patterns for the CEG basalts (low-Ti, medium continuous lines; high-Ti, fine continuous lines). Additional data illustrated are high-Ti lavas from Andreasen *et al.* (2004) (grey shaded region), average Theistareykir composition (triangles) calculated from the dataset of Stracke *et al.* (2003), using analyses with MgO between 10 and 15 wt %, $La/Yb_{(N)} < 1$ and excluding the Draugarhraun and Asbyrgi basalts, and average Atlantic MORB (circles) with $La_N/Sm_N < 1$ from Arevalo & McDonough (2010). Element order after Stracke *et al.* (2003); normalizing values from McDonough & Sun (1995).

$^{206}Pb/^{204}Pb = 17{\cdot}59–18{\cdot}32$, $^{207}Pb/^{204}Pb = 15{\cdot}36–15{\cdot}44$ and $^{208}Pb/^{204}Pb = 37{\cdot}59–38{\cdot}13$ (Fig. 6). Pb isotope compositions are less radiogenic than contemporaneous uncontaminated high-Ti lavas; however, contamination tends to shift these lavas to less radiogenic compositions so that there is considerable overlap. Notably, the sample with an elevated Ba content (404250) does not show isotopic evidence for being strongly contaminated, indicating that leaching was efficient in removing any remnant secondary material in vesicles. The CEG and FI low-Ti basalts have virtually identical compositions in Sr–Nd–Hf–Pb isotope space, although a few FI samples extend to more radiogenic Sr compositions and several extend to lower $^{87}Sr/^{86}Sr$ and have Pb isotopic compositions closer to the NHRL. The five high-Ti samples examined have $^{87}Sr/^{86}Sr = 0{\cdot}70315–0{\cdot}70333$, $\varepsilon_{Nd(i)} = +6{\cdot}6$ to $+7{\cdot}1$, $\varepsilon_{Hf(i)} = +11{\cdot}1$ to $+12{\cdot}2$, $^{206}Pb/^{204}Pb = 18{\cdot}27–18{\cdot}52$, $^{207}Pb/^{204}Pb = 15{\cdot}42–15{\cdot}46$ and $^{208}Pb/^{204}Pb = 38{\cdot}16–38{\cdot}37$, in agreement with the more comprehensive datasets presented by Peate & Stecher (2003), Andreasen *et al.* (2004) and Barker *et al.* (2006), as well as those from the FI (Søager & Holm, 2009, 2011).

Hart (1984) quantified vertical deviations in $^{207}Pb/^{204}Pb$ and $^{208}Pb/^{204}Pb$ from the Northern Hemisphere Reference Line (NHRL) with the parameters $\Delta^{207}Pb$ $\{[^{207}Pb/^{204}Pb - (0{\cdot}1084\,^{206}Pb/^{204}Pb + 13{\cdot}491)] \times 100\}$ and $\Delta^{208}Pb$ $\{[^{208}Pb/^{204}Pb - (1{\cdot}209\,^{206}Pb/^{204}Pb + 15{\cdot}627)] \times 100\}$, respectively. All CEG basalts in this study are characterized by negative $\Delta^{207}Pb$ (low-Ti $= -1{\cdot}9$ to $-5{\cdot}4$,

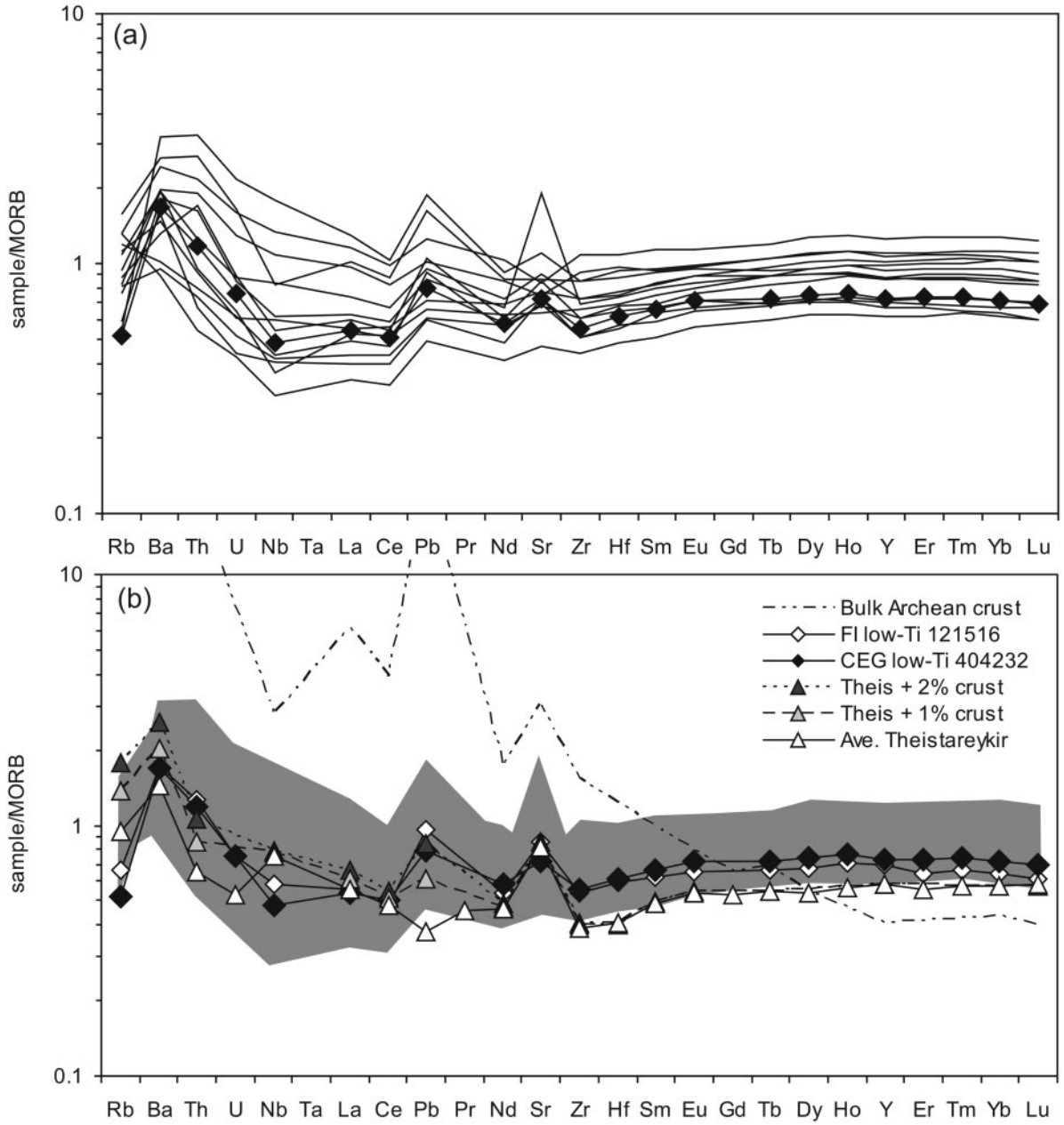

Fig. 5. N-MORB-normalized extended multi-element diagrams, normalized to the values of Arvelo & McDonough (2010). (a) CEG low-Ti samples; the high-Ba sample (404250) is excluded; filled diamonds relate to a representative low-Ti sample (404232, approximating a primary melt). (b) Comparison between 404232, an average Theistareykir composition from Stracke *et al.* (2003) (see Fig. 4) and an analysis from the FI low-Ti lavas (from Søager & Holm, 2011). The shaded field represents the full low-Ti dataset as shown in (a). Also shown are the effects of contamination of an average Theistareykir composition with 1 and 2% bulk Archean crust [crust composition from Wedepohl *et al.* (1991)].

high-Ti = −3·9 to −5·3) and positive Δ^{208}Pb (low-Ti: +26 to +114, high-Ti = +35 to +47); that is, having $^{207}Pb/^{204}Pb$ and $^{208}Pb/^{204}Pb$ compositions that plot, respectively, above and below the NHRL. These signatures are also characteristic of both modern Iceland plume compositions (e.g. Thirlwall *et al.*, 2004) and other proto-Iceland plume compositions [e.g. CEG (Barker *et al.*, 2006; this study), FI (Søager & Holm, 2011), West Greenland (Larsen & Pedersen, 2009) and Baffin Island (Jackson *et al.*, 2010)]. Although age correction has a relatively large effect on Pb isotopic compositions in the CEG, it has little effect on these characteristic offsets from the NHRL. Calculation of Δ^{207}Pb and Δ^{208}Pb using age-corrected data and recalculation of the NHRL to 55

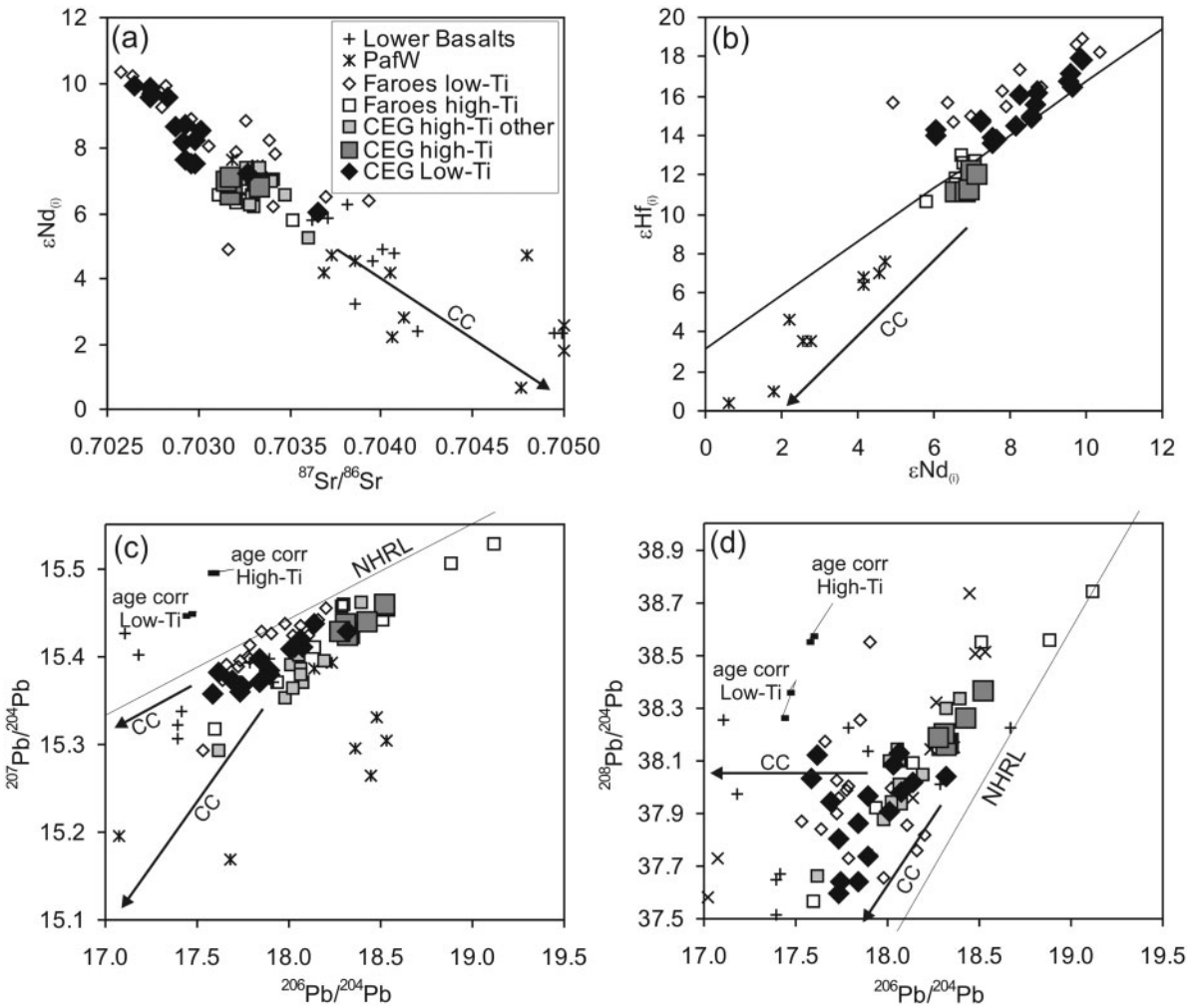

Fig. 6. Isotope compositions of CEG low-Ti basalts compared with contemporaneous magmas in East Greenland and the Faroe Islands. (a) $^{87}Sr/^{86}Sr$ vs $\varepsilon Nd_{(i)}$; (b) $\varepsilon Nd_{(i)}$ vs $\varepsilon Hf_{(i)}$; (c) $^{206}Pb/^{204}Pb$ vs $^{207}Pb/^{204}Pb$; (d) $^{206}Pb/^{204}Pb$ vs $^{208}Pb/^{204}Pb$. Comparative data are shown from Hansen & Nielsen (1999), Peate *et al.* (2003), Andreasen *et al.* (2004) and Søager & Holm (2011). Arrows labelled CC represent general trends of crustal contamination as observed in the Lower Basalts and Prinsen af Wales Bjerge Formation (PafW). Vectors on the Pb isotope diagrams represent the maximum and minimum change for the high- and low-Ti basalts with age correction to 55 Ma. NHRL, Northern Hemisphere Reference Line.

Ma, assuming the depleted mantle U–Th–Pb concentrations estimates of Salters & Stracke (2004), results in 'age-corrected' $\Delta^{207}Pb$ values for the low-Ti basalts that are on average 0·5 units less negative and $\Delta^{208}Pb$ values that are on average 0·8 units less positive compared with the measured values.

Comparison of the isotopic compositions of the CEG low-Ti lavas (source-corrected where appropriate) with Iceland shows general overlaps, in particular with depleted compositions from Theistareykir and the surrounding ridges (Kolbeinsey and Reykjanes) (Fig. 7). However, some differences are apparent. The low-Ti basalts overlap with Iceland but extend to less radiogenic Sr in a plot of $^{87}Sr/^{86}Sr$ vs $\varepsilon Nd_{(s.c.)}$ to overlap with the adjacent ridges (Reykjanes and Kolbeinsey). The low-Ti basalts also tend to be offset to somewhat less radiogenic Sr at a given Nd isotopic composition, a feature also noted for the ridges adjacent to Iceland by Thirlwall *et al.* (2004). Age or source correction issues for the low-Ti samples will only emphasize these offsets from Theistareykir. There is near-total overlap between Iceland and adjacent ridges and the low-Ti lavas in Hf–Nd isotopic space (Fig. 7). In a plot of $^{206}Pb/^{204}Pb$ vs $^{207}Pb/^{204}Pb$ the low-Ti lavas overlap with Theistareykir and extend to less radiogenic compositions, and tend to have lower $^{207}Pb/^{204}Pb$ at a given $^{206}Pb/^{204}Pb$ than the Reykjanes and Kolbeinsey ridges (Fig. 7), whereas both the low-Ti and high-Ti lavas are offset to lower $^{206}Pb/^{204}Pb$ at a given $^{208}Pb/^{204}Pb$ compared with Iceland and surrounding ridges (see also Barker *et al.*, 2006; Søager & Holm, 2009, 2011). The offset in $^{208}Pb/^{204}Pb$ is

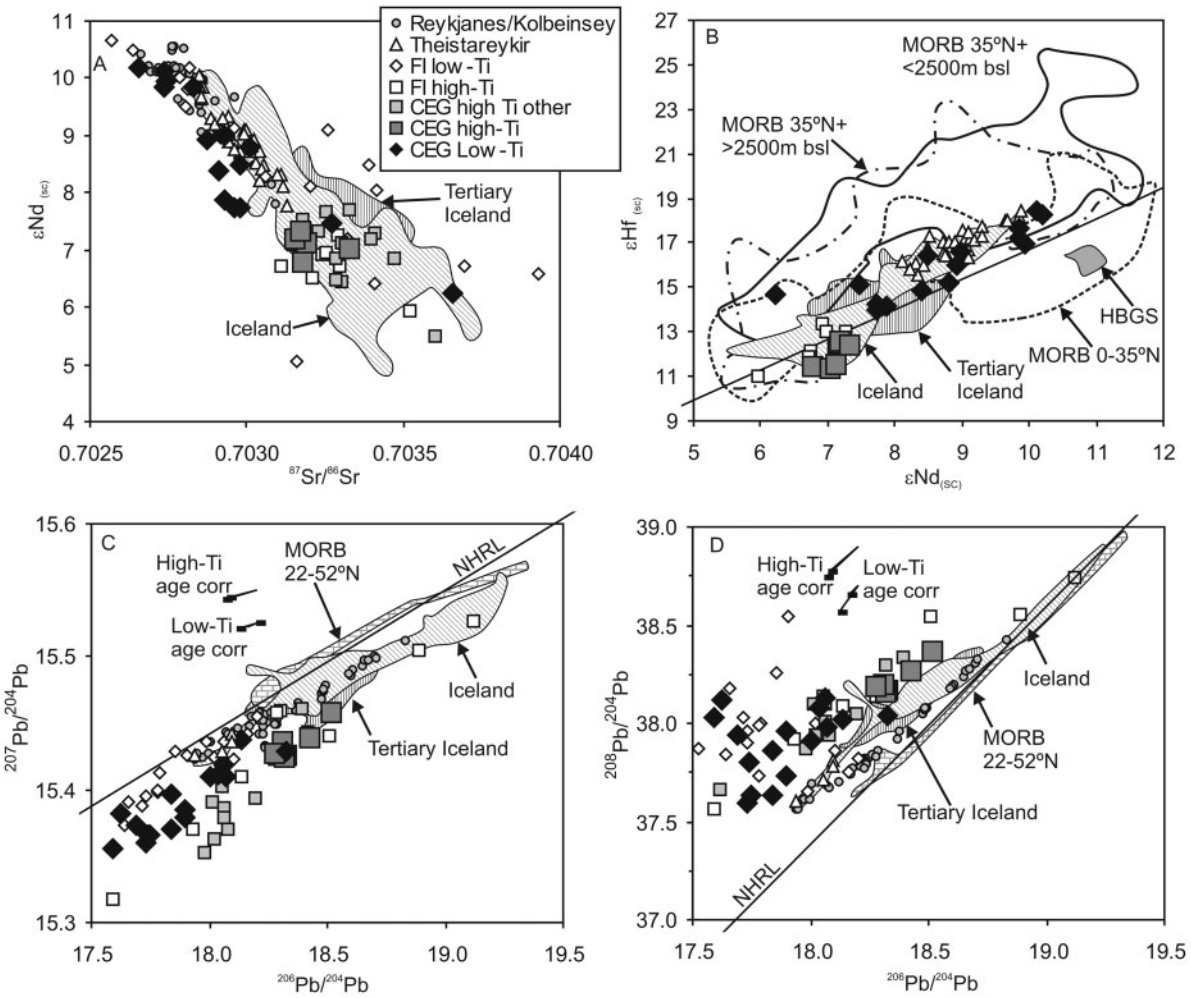

Fig. 7. Source-corrected isotope compositions of CEG and Faroe Islands basalts compared with selected modern-day compositions from Iceland and adjacent ridges. (a) $^{87}Sr/^{86}Sr$ vs $\varepsilon Nd_{(sc)}$; (b) $\varepsilon Nd_{(sc)}$ vs $\varepsilon Hf_{(sc)}$ with the ocean island basalt correlation line of Johnson & Beard (1993); (c) $^{206}Pb/^{204}Pb$ vs $^{207}Pb/^{204}Pb$; (d) $^{206}Pb/^{204}Pb$ vs $^{208}Pb/^{204}Pb$ [only Pb double-spike data are used in (c) and (d)]. Data from Stracke *et al.* (2003), Andres *et al.* (2004), Thirlwall *et al.* (2004), Agranier *et al.* (2005), Blichert-Toft *et al.* (2005), Debaille *et al.* (2006), Kokfelt *et al.* (2006), Kitagawa *et al.* (2008), Søager & Holm (2009, 2011) and Peate *et al.* (2009, 2010). Vectors on the Pb isotope diagrams represent the maximum and minimum change for the high- and low-Ti basalts with age correction to 55 Ma. bsl = below sea level; HBGS = Hatton Bank & Goban Spur (from Kempton *et al.* (2000)

not due to age correction effects, as this tends to move compositions parallel to the NHRL, rather than perpendicular to it.

DISCUSSION

In the following discussion, we assess the effects of crystal fractionation, partial melting and crustal contamination, and conclude that at least two mantle source components, plus small degrees of crustal contamination, are required to explain the observed geochemical variations of the CEG low-Ti basalts. We compare the CEG compositions with previously postulated mantle components in the North Atlantic using both trace element and isotopic constraints and conclude that the depleted component(s) in CEG were similar to depleted sources currently tapped under modern Iceland and the adjacent oceanic ridges, yet display some subtle differences suggesting that these plume sources may have varied with time. We argue that these depleted components are distinct from typical global N-MORB sources and were an integral part of the Iceland mantle plume.

Crystal fractionation

The low-Ti basalts have MgO contents varying from 17·3 to 7·0 wt % and Ni contents that vary from 735 to 67 ppm; they show similar overall trends in major and trace element compositions to basalts from Theistareykir

(Stracke *et al.*, 2003). Momme *et al.* (2006) proposed that the parental melts of the low-Ti basalts had MgO = 13·6 wt % and 460 ppm Ni. Similarly, Stracke *et al.* (2003) argued for a primary melt with *c.* 14 wt % MgO at Theistareykir. Recent modelling of the contemporaneous low-Ti magmas on the Faroe Islands by Søager & Holm (2011) suggests parental melts with 16–19% MgO and high potential mantle temperatures of 1475–1550°C. Despite these variations, it is apparent that most of the CEG low-Ti basalts do not represent primary magmas; most are more evolved and several have apparently undergone olivine accumulation (see Fig. 2). The observed variations in REE can be attributed to fractional crystallization of olivine, clinopyroxene and plagioclase, although it is likely that varying degrees of melting also played a large role in controlling the REE budget, as discussed in more detail below.

Partial melting processes

In a plot of La/Yb_N vs Dy/Yb_N (Fig. 8) the low-Ti basalts display a trend that contrasts markedly with the largely invariant and lower Dy/Yb_N observed in depleted compositions from Iceland and adjacent ridges. Aggregated non-modal melting trajectories (Shaw, 1970) for both spinel- and garnet-facies sources are presented in Fig. 8. We note that fractional crystallization of an assemblage of olivine, pyroxene and plagioclase will result in insignificant changes in Dy/Yb_N and La/Yb_N. Use of typical depleted MORB mantle (e.g. Workman & Hart, 2005) as a source is inappropriate for both CEG and Iceland compositions, primarily as a consequence of their relatively low La/Yb_N; instead, we construct these models using a depleted MORB mantle source that has previously had a small degree of melt removed in the spinel facies (see also Momme *et al.*, 2006). Previous studies have shown that magmas from most flood basalt provinces typically do not plot on or near spinel- or garnet-facies melting trajectories. The observed trends can be explained by mixing of melts derived from both lithologies (e.g. Thirlwall *et al.*, 1994, 2000; Baker *et al.*, 1997). The observed variations in the low-Ti basalts are broadly consistent with mixing of small-degree melts (1–3%) from the garnet facies with relatively large-degree melts (20%) from the spinel facies. We note that these trends are consistent whether we plot REE-ID or ICP-MS REE data. On the basis of the modelling presented in Fig. 8, *c.* 20–30% of the melt is derived from garnet-facies mantle. This contrasts with the assumptions of Momme *et al.* (2006) that the low-Ti basalts were derived entirely from spinel-facies mantle. There is no correlation between Dy/Yb_N and $^{143}Nd/^{144}Nd$ ($r^2 = 0{\cdot}02$, not shown) in the low-Ti basalts as would be expected if a more enriched component was preferentially tapped at greater depths (i.e. in the stability field of garnet). Similar processes of polybaric melt

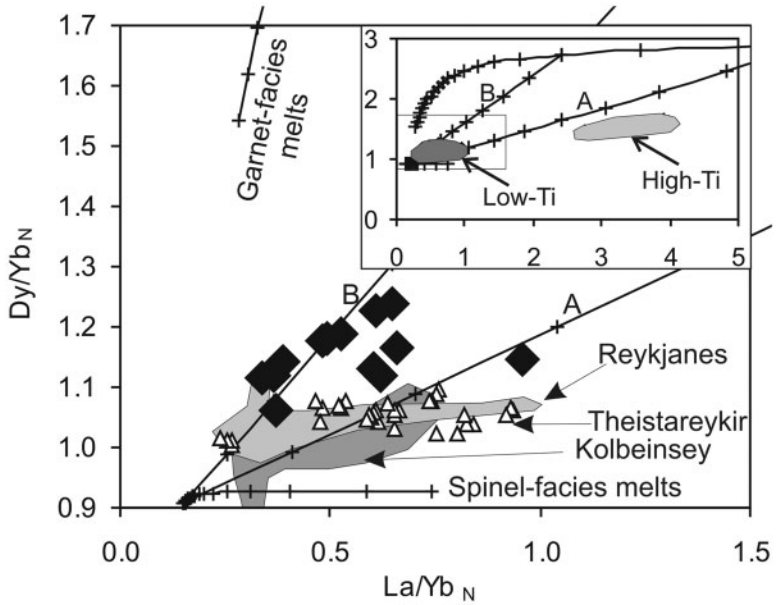

Fig. 8. Variation of La/Yb_N vs Dy/Yb_N for CEG low-Ti basalts (filled diamonds) and Theistareykir basalts ($La/Yb_N < 1$; data from from Stracke *et al.* 2003) (open triangles). Shaded fields represent data from the Reykjanes Ridge from Murton *et al.* (2002) (restricted to latitudes 57–61°N to exclude influence of the Iceland plume) and from the Kolbeinsey Ridge from Devey *et al.* (1994). Aggregated non-modal melting curves for a depleted MORB mantle source (Workman & Hart, 2005), previously depleted by removal of 0·5% melting in the spinel facies, in the garnet and spinel facies are shown, together with mixing curves between 1% (A) and 3% (B) melting in the garnet facies and 20% melting in the spinel facies. Tick marks represent 1% melting (up to 20%) and 10% mixing. Curves calculated using partition coefficients presented by Stracke *et al.* (2003) and parameters presented by Thirlwall *et al.* (1994). Crustal contamination by average continental crust will result in a small increase in La/Yb_N (*c.* 0·1) but no significant change in Dy/Yb_N.

aggregation have been proposed for both the CEG high-Ti basalts (e.g. Tegner *et al.*, 1998*a*; Momme *et al.*, 2006) and the modern Iceland plume (e.g. Stracke *et al.*, 2003; Maclennan, 2008). However, it is clear that the proportion of melt derived from the garnet facies is greater in the low-Ti basalts from the CEG than for similar depleted compositions from modern Iceland. This may be a consequence of a potentially hotter mantle plume combined with the presence of a thicker lithospheric lid, restricting continued melting of spinel-facies mantle at shallower depths.

Role of crustal contamination and identifying discrete mantle sources

Isotopic evidence for crustal contamination is widespread in East Greenland (Fram & Lesher, 1997; Fitton *et al.*, 1997, 2000, 2003; Saunders *et al.*, 1997; Hansen & Nielsen, 1999; Peate *et al.*, 2003) (see Fig. 7). Crustal contamination is less evident in the high-Ti Plateau Basalts (e.g. Peate & Stecher, 2003; Andreasen *et al.*, 2004; Barker *et al.*, 2006), allowing many compositions to be treated as uncontaminated. However, the relatively low Pb (<1 ppm), Nd (<4 ppm) and Hf (<2 ppm) contents of the low-Ti basalts makes them considerably more susceptible to contamination than the high-Ti basalts, which has important implications for identifying potential mantle source components and for making comparisons with modern Icelandic compositions.

CEG crust is dominated by Archean gneisses reworked during the Proterozoic (Leeman *et al.*, 1976; Taylor *et al.*, 1992; Kalsbeek *et al.*, 1993). The basement is characterized by low εNd (−15 to −41), variable $^{87}Sr/^{86}Sr$ (0·703–0·755) and unradiogenic $^{206}Pb/^{204}Pb$ (<16) owing to removal of Rb and U during Archean metamorphism (Weaver & Tarney, 1981). Two Archean crustal contaminants are identified in CEG, a granulite-facies ($^{87}Sr/^{86}Sr = 0{\cdot}703$–$0{\cdot}718$, low $^{208}Pb/^{204}Pb$) and an amphibolite-facies ($^{87}Sr/^{86}Sr = 0{\cdot}738$–$0{\cdot}755$, high $^{208}Pb/^{204}Pb$) component, both with low $^{206}Pb/^{204}Pb$ (13·4–15·9) and εNd (*c.* −15 to −40) (e.g. Leeman *et al.*, 1976; Taylor *et al.*, 1992; Kalsbeek *et al.*, 1993). Crustal contamination in the NAIP results in higher $^{87}Sr/^{86}Sr$, lower εNd and especially lower $^{206}Pb/^{204}Pb$ (e.g. Hansen & Nielsen, 1999; Kempton *et al.*, 2000; Peate & Stecher, 2003; Peate *et al.*, 2003, 2008; Andreassen *et al.*, 2004; Riishuus *et al.*, 2005). In contaminated high-Ti samples, scatter in Pb isotopic compositions indicates that both amphibolitic and granulitic compositions were involved at different levels in the crust (Andreasen *et al.*, 2004; Barker *et al.*, 2006; Peate *et al.*, 2008). Crustal contamination complicates the identification of mantle end-members, therefore we now examine the potential consequences of crustal contamination in detail using both isotopic compositions and trace element data.

Combined trace element and isotopic constraints on contamination and sources

High degrees of crustal contamination in East Greenland and Faroe Island basalts have been identified through their increased SiO_2 contents, and elevated ratios of large ion lithophile elements (LILE) or LREE relative to high field strength elements (HFSE), such as K/Nb and La/Nb (e.g. Peate *et al.*, 2008). However, no such correlations are observed between isotopic compositions and silica contents in the CEG low-Ti dataset.

Pb is highly sensitive to crustal contamination, and therefore the offsets observed in Pb isotopic space between the CEG low-Ti basalts and North Atlantic MORB, the NHRL and depleted Icelandic lavas (e.g. Fig. 7), combined with the positive Pb peaks in MORB-normalized trace element plots (Fig. 5) could be indicative of small, yet ubiquitous, amounts of crustal contamination of magmas derived from similar mantle sources to modern depleted North Atlantic compositions (e.g. Theistareykir or oceanic ridges adjacent to Iceland). In Fig. 5 we illustrate that small degrees of crustal contamination (1–2%) of a depleted Iceland basalt composition (e.g. Theistareykir) could produce trace element compositions similar to a typical CEG low-Ti basalt and replicate the positive Pb peak and generally higher Th contents. A broad trend of decreasing $^{206}Pb/^{204}Pb$ with decreasing Ce/Pb in the CEG low-Ti basalts is also observed, broadly consistent with small degrees of crustal contamination; however, we also note that the relationship with $^{87}Sr/^{86}Sr$ and Nd isotopes is less clear (Fig. 9). It is important to note that crustal contamination of a depleted Iceland basalt or MORB-like composition cannot explain the relatively low Nb contents of the CEG low-Ti basalts, and this therefore must be a distinctive characteristic of the source. If the positive Pb peak seen in the MORB-normalized CEG low-Ti basalts is solely a consequence of contamination, this would imply that they are all ubiquitously contaminated to small yet varying degrees. Uncontaminated parental magmas should therefore have even less radiogenic $^{87}Sr/^{86}Sr$, and higher εNd and $^{206}Pb/^{204}Pb$ than observed. For example, a representative CEG low-Ti sample (404241) with low $^{87}Sr/^{86}Sr$ (0·7027) and high $^{206}Pb/^{204}Pb$ (18·134), indicative of minimal contamination, has $Pb/Pb^* = 1{\cdot}3$. In terms of Pb concentrations alone, such a Pb peak is equivalent to *c.* 1·5% contamination of a Theistareykir-like composition. In terms of isotopic compositions this would imply an uncontaminated parent with very unradiogenic $^{87}Sr/^{86}Sr$ (*c.* 0·7022) yet relatively radiogenic $^{206}Pb/^{204}Pb$ (*c.* 20), an unknown composition in the North Atlantic. Although less extreme, such arguments remain relevant if a MORB-like parent with $Pb/Pb^* = 1$ is used. Acknowledging the analytical challenges associated with the determination of relatively low Pb concentrations and the potential for contamination during sample processing, we

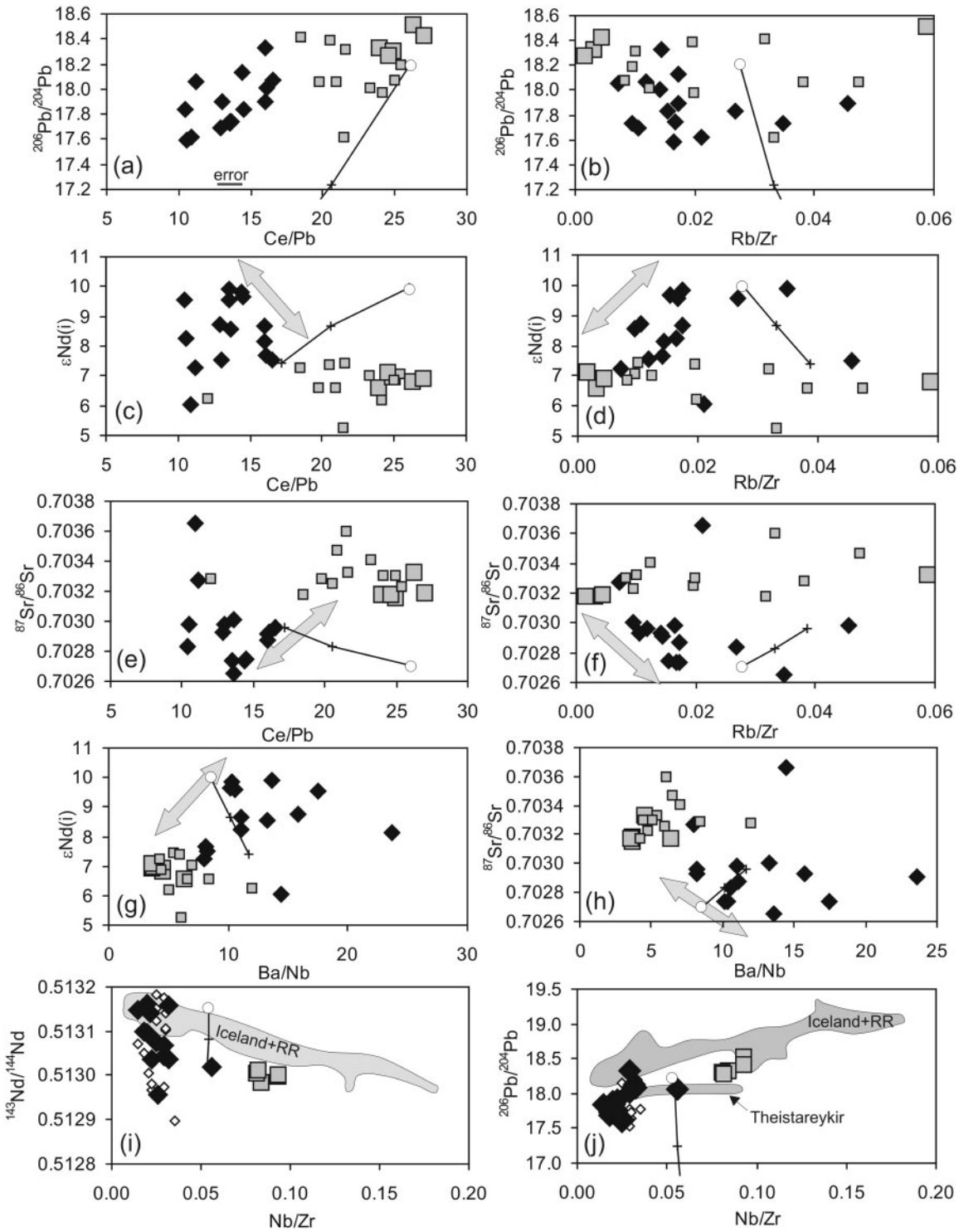

Fig. 9. Selected trace element ratios vs isotopic composition. Grey arrows represent the variation induced by contributions from different depleted mantle sources; the vectors illustrate the effects of small degrees of crustal contamination, modeled as contamination of an average Theistareykir composition (open circle) by average Greenland Archean crust (Wedepohl *et al.*, 1991) with $^{87}Sr/^{86}Sr = 0{\cdot}71$, $^{143}Nd/^{144}Nd = 0.511$ ($\varepsilon Nd = -32$) and $^{206}Pb/^{204}Pb = 15$; tick marks represent 0·5% contamination. Fields for Iceland and the Reykjanes Ridge (Iceland + RR) and Theistareykir in the Nb/Zr plots are from Thirlwall *et al.* (2004). Black diamonds, CEG low-Ti; open diamonds, FI low-Ti; large grey squares, CEG high-Ti (this study); small grey squares, CEG high-Ti (Andreasen *et al.* 2004). The reproducibility of trace element ratios based on replicate analyses of standards (Supplementary Data Appendix A) is smaller than the symbol size used with the exception of Ce/Pb (reproducibility = ±10% 2 SD).

tentatively suggest that the positive Pb peak in part represents a characteristic feature of the CEG low-Ti basalts. More detailed, high-quality Pb concentration data from the FI are needed to confirm if this is also the case there.

Evidence for at least two distinct mantle components, as well as for small degrees of crustal contamination in the CEG low-Ti lavas can be seen in Fig. 9, where trace element ratios that change significantly with crustal contamination yet are unaffected by fractional crystallization and melting processes (e.g. Rb/Zr, Ba/Nb, Ce/Pb) are plotted against isotopic composition. The diagrams can be interpreted in terms of the involvement of four end-members—two mantle components and both amphibolitic and granulitic crust. The main compositional variations in the CEG low-Ti basalts appear to be between two main depleted magmatic components—one of which is a depleted component with unradiogenic $^{87}Sr/^{86}Sr$, radiogenic Nd, high Rb/Zr and Ba/Nb, and relatively low Ce/Pb, whereas the other is slightly less depleted with more radiogenic Sr, less radiogenic Nd, lower Rb/Zr and Ba/Nb, and higher Ce/Pb. This second component has an isotopic composition similar to the CEG high-Ti basalts, but has depleted characteristics. We note that these variations primarily reflect correlations between HFSE and isotopic compositions, whereas the LILE (e.g. Rb, Ba, Pb) remain relatively constant with changing isotopic compositions. In general, the spread in compositions between these components in trace element–Sr–Nd isotope space trends at a relatively high angle to that expected from crustal contamination, allowing their identification. However, some scatter in these diagrams is consistent with small degrees (generally <1%) of contamination by both amphibolitic and granulitic crustal components in a number of the samples. Distinguishing mixing between the two mantle-derived components and the effects of crustal contamination in Pb isotope space is less clear, primarily as crustal contamination has a much larger effect on the Pb isotopic compositions and masks the primary signals.

We note that correlations between Rb/Zr, Ba/Nb and Ce/Pb and isotopic composition in the CEG high-Ti basalts are either minor or absent, primarily because these basalts are less susceptible to contamination owing to their generally higher trace element concentrations. Instead, the CEG high-Ti basalts appear to indicate input from sources with, for example, both low and high Rb/Zr but little variation in isotopic composition. A broad trend is observed in the low-Ti basalts with relatively low $^{87}Sr/^{86}Sr$ and radiogenic Nd towards higher Rb/Zr, which could be interpreted as crustal contamination (this low-Ti end-member will have lower Zr and therefore be more susceptible to contamination) or involvement of the high Rb/Zr high-Ti component.

Plots of Nb/Zr vs $^{206}Pb/^{204}Pb$ and $^{143}Nd/^{144}Nd$ illustrate that the most depleted CEG and FI low-Ti basalts overlap with the most depleted compositions from the North Atlantic (Fig. 9), yet both FI and CEG show a trend that is clearly divergent from that seen on Iceland and adjacent ridges, extending to less radiogenic compositions at relatively constant Nb/Zr. These variations are consistent with small degrees of crustal contamination. The amounts of contamination indicated do not agree between Nd (2–3%) and Pb isotopes (<0·5%), although this is highly dependent on the elemental concentrations chosen for the end-members in the modelling. It is apparent that the uncontaminated low-Ti parent melts apparently had a much more limited range in Nb/Zr than in the modern North Atlantic, and there is, for example, little evidence for involvement of the low $^{143}Nd/^{144}Nd$–high Nb/Zr enriched plume components observed on Iceland (e.g. IE1 and IE2 of Thirlwall *et al.*, 2004; enriched components with relatively high and low $^{206}Pb/^{204}Pb$ respectively). Alternatively, this variation may also reflect a high $^{143}Nd/^{144}Nd$ and low Nb/Zr source that is not preserved in the modern North Atlantic, although we stress that we cannot distinguish this option from crustal contamination. This is potentially also suggested by the contemporaneous CEG high-Ti basalts, which have lower Nb/Zr than Icelandic compositions at equivalent $^{143}Nd/^{144}Nd$, and other trace element ratio–isotope plots that indicate a trend towards high-Ti compositions. A single Iceland sample (RP103A) presented by Thirlwall *et al.* (2004) plots within the CEG low-Ti field in a plot of Nb/Zr vs $^{143}Nd/^{144}Nd$. This sample is distinct from the CEG low-Ti lavas and characterized by positive $\Delta^{207}Pb$ and negative ΔNb, and defines the probably volumetrically minor ID2 component of Thirlwall *et al.* (2004) for which there is no evidence in our dataset.

Identification of primitive basalt end-members for crustal contamination modelling is non-trivial given evidence for multiple mantle end-members in the North Atlantic Province (e.g. Fig. 9 and Søager & Holm, 2011) and modern Iceland (Thirlwall *et al.*, 2004). We model crustal contamination using two potential depleted end-members. The first component used in contamination modelling is CEG low-Ti sample 404290, which has the highest $^{206}Pb/^{204}Pb$ in the dataset, and is therefore potentially most representative of the less depleted component identified above. We use one of the depleted components suggested for the Faroe Islands—the Faroes Depleted Component (FDC) of Søager & Holm (2011)—as the more depleted end-member. The FDC bears many similarities to North Atlantic MORB and is broadly similar to the ID1 (a depleted component best seen at Theistareykir) and RRD1 (the depleted component on the Reykjanes Ridge) end-members, which dominate the depleted magmatism on Iceland (Thirlwall *et al.*, 2004). All three components are distinguished from MORB (e.g. south of the Charlie–Gibbs Fracture Zone) by having negative $\Delta^{207}Pb$ (Fig. 10). A plot of $^{208}Pb/^{204}Pb$ vs

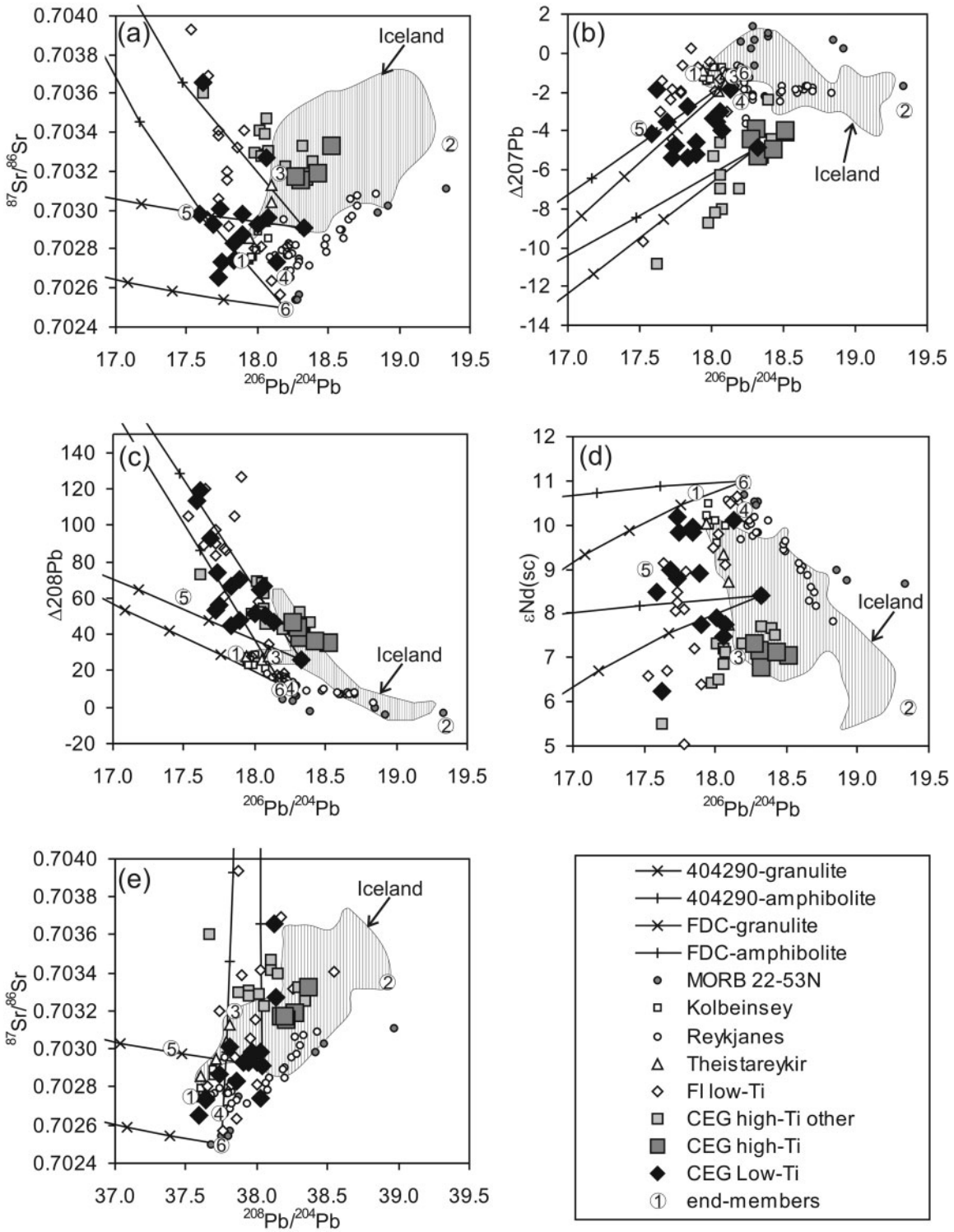

Fig. 10. Selected Sr–Nd–Pb isotope plots illustrating the effects of small degrees of crustal contamination (via bulk mixing) of magmas derived from the FDC end-member [assuming elemental concentrations equivalent to the average N-MORB concentrations of Arevalo & McDonough (2010)] and sample 404290. Average granulitic and amphibolitic contaminants used are from the data of Riishuus *et al.* (2005), assuming $\Delta^{207}Pb$ that is the same as the virtually identical average Lewisian gneisses presented by Dickin (1981). Tick marks represent 0·5% increments of contamination. Additional high-Ti data (small squares) are from Andreasen *et al.* (2004) and Barker *et al.* (2006). Data from Iceland and adjacent ridges (double spike only) are from Thirlwall *et al.* (2004) and Peate *et al.* (2009, 2010). Also shown are selected mantle end-member components identified by Thirlwall *et al.* (2004) [(1) IDl; (2) IEl; (3) IE2; (4) RRDl], Ellam & Stuart (2000) [(5) NAEM] and Søager & Holm (2011) [(6) FDC].

$^{87}Sr/^{86}Sr$ shows that the CEG (and FI) low-Ti compositions trend towards a component with less radiogenic Sr and lower $^{208}Pb/^{204}Pb$ than observed in the most depleted compositions on Iceland (Theistareykir), indicating involvement of a depleted component similar to ID1 or FDC (Fig. 10). This plot also shows a broad positive trend between $^{208}Pb/^{204}Pb$ and $^{87}Sr/^{86}Sr$ that parallels that of other NAIP magma series and indicates involvement of a second mantle-derived component perhaps similar in composition to sample 404290. Contamination models are calculated assuming elemental concentrations for the FDC equivalent to the average N-MORB concentrations of Arevalo & McDonough (2010). This is a minimum estimate, as the CEG low-Ti basalts typically have lower concentrations of Pb, Sr and Nd than N-MORB (e.g. Fig. 5). We emphasize that these are models only, and that significant isotopic and trace element heterogeneity is likely in the mantle-derived and especially the crustal end-members. We note that the actual depleted component(s) involved may have been even more depleted, given the likelihood that the depleted mantle end-members may not be accurately reflected in the resultant melts (e.g. Stracke & Bourdon, 2009).

The range of isotopic compositions observed in the low-Ti basalts is inconsistent with a simple scenario of contamination of a melt derived from a unique low-Ti source by a single homogeneous crustal component. Instead, a range of mantle source compositions and/or multiple contaminants are implied. Modelling indicates that the isotopic compositions of the low-Ti basalts can be attributed to contributions from a broadly 'MORB-like' depleted component similar to FDC or the ID1 or RRD components of Thirlwall *et al.* (2004) and a slightly less depleted component with higher $^{208}Pb/^{204}Pb$ and $^{206}Pb/^{204}Pb$, more negative $\Delta^{207}Pb$, and lower $^{87}Sr/^{86}Sr$ and $^{143}Nd/^{144}Nd$. This latter component has isotopic compositions not dissimilar to the high-Ti CEG basalts, and does not appear to be present under modern-day Iceland. A crude correlation between increasing Nb/Zr and decreasing Ba/Nb (not shown) lends credence to the suggestion that the distinct trend in Nb/Zr vs $^{143}Nd/^{144}Nd$ seen in the low-Ti basalts (Fig. 9) is due to this component rather than crustal contamination. We tentatively suggest that this component may reflect involvement of melts derived from re-melting of residual material from the high-Ti source, depleted during deeper melting and removal of the high-Ti magmas. This would explain the trends towards isotopic compositions similar to the high-Ti magmas, but retention of relatively depleted trace element compositions. For example, such a residue would be expected to have lower Nb/Zr than the high-Ti basalts, but a similar Nd isotopic composition. These melts underwent small degrees of crustal contamination (typically less than 0·5%) by granulitic and/or amphibolite contaminants. The result is a broad spread to less radiogenic uranogenic Pb, more negative $\Delta^{207}Pb$ and more positive $\Delta^{208}Pb$, and lower $^{87}Sr/^{86}Sr$, as is also consistent with contamination histories observed in the contemporaneous high-Ti basalts (Andreasen *et al.*, 2004).

Offsets from the NHRL are critical to distinguishing North Atlantic components from global MORB, and have been used to argue for the involvement of relatively young (Palaeozoic) recycled basaltic oceanic crust in the Iceland plume (Thirlwall *et al.*, 2004). However, these parameters are particularly susceptible to contamination as typical crustal compositions in CEG have extremely negative $\Delta^{207}Pb$ (−12 to −30) and positive $\Delta^{208}Pb$ (120–450). Trends to more negative $\Delta^{207}Pb$ (−6+), positive $\Delta^{208}Pb$ (80+), increasing $^{87}Sr/^{86}Sr$ and decreasing $^{206}Pb/^{204}Pb$ with contamination are observed in the high-Ti lava series (Andreasen *et al.*, 2004; Barker *et al.*, 2006). Small degrees of crustal contamination can also explain the range of $\Delta^{207}Pb$ and $\Delta^{208}Pb$ in the low-Ti basalts to compositions more extreme than observed on Iceland (Fig. 10). However, even uncontaminated high-Ti CEG basalts appear to have more extreme offsets from the NHRL than Iceland (Barker *et al.*, 2006) and this is considered to be an integral feature of CEG high-Ti magmatism that distinguishes it from modern Icelandic magmas.

The FI low-Ti basalts show similar variations to the CEG low-Ti basalts in all isotopic diagrams (Fig. 10). The FI lavas were emplaced through thick continental crust equivalent to that found in East Greenland and therefore much of their isotopic variation could also be potentially explained by small degrees of crustal contamination as suggested here. Søager & Holm (2011) argued that most of their dataset was uncontaminated, in part referring to low Th/U and Th/Nb in the CEG dataset of Barker (2006), which we have found to be inaccurate. On the basis of the assumption that their samples were uncontaminated, Søager & Holm (2011) argued that the low $^{206}Pb/^{204}Pb$ depleted North Atlantic End-Member (NAEM) component of Ellam & Stuart (2000) was an important component during magmatism in the Faroe Islands. Our modelling demonstrates that trends towards this component can also be adequately explained by minor (<1%) amounts of crustal contamination. Ascertaining degrees of contamination is dependent on which model is used. Using assimilation–fractional crystallization (AFC)-type models, as done by Søager & Holm (2011), to model assimilation will tend to underestimate the degree of contamination compared with bulk mixing, especially when relatively low values of r (rate of assimilation to crystallization) are used. Primitive hot magmas in flood basalt provinces may assimilate significant amounts of crust during turbulent magma migration without undergoing significant crystallization (e.g. Huppert & Sparks, 1985) and therefore bulk-mixing modelling is potentially more

appropriate. Furthermore, it has been suggested that hot basaltic systems crystallizing primarily olivine may have *r* values approaching unity or greater (Reiners *et al.*, 1995) and therefore will result in AFC models that mimic bulk mixing. Søager & Holm (2011) also identified a trend of FI samples with $\varepsilon Nd < +9$ towards more radiogenic Pb and positive $\Delta^{207}Pb$, which they interpreted as representing the involvement of a component similar to the Icelandic Öræfajökull lavas and the ID2 component of Thirlwall *et al.* (2004), which may represent a pelagic sediment component. If such a trend is present in the CEG low-Ti dataset, it is obscured by the scatter caused by crustal contamination.

Mantle sources: depleted plume mantle or a depleted MORB mantle source?

Combined trace element and isotopic characteristics (Fig. 9) suggest that two distinct mantle sources are involved in the genesis of the CEG low-Ti basalts. We are hesitant to name these components given the plethora of acronyms already proposed for mantle components in the North Atlantic Igneous Province (e.g. Hanan & Schilling, 1997; Thirlwall *et al.*, 2004; Kokfelt *et al.*, 2006; Kitagawa *et al.*, 2008; Søager & Holm, 2011). We also note that the FDC component bears a striking resemblance to typical MORB and the RRD1 component that dominates depleted magmatism to the south of Iceland, as well as the ID1 component most evident at Theistareykir (Thirlwall *et al.*, 2004). Thirlwall *et al.* (2004) have suggested that a mixture dominated by RRD1, together with the ID1 and ID2 components, represents the main depleted component on Iceland, and it would appear that a broadly similar component may also have existed in CEG at 55 Ma.

There has been considerable debate as to the physical location and origin of the depleted component(s) with respect to the Iceland mantle plume, primarily divided into arguments suggesting that it represents ambient depleted North Atlantic upper mantle incorporated into the plume at shallow levels (e.g. Hanan *et al.*, 2000; Stracke *et al.*, 2003), or that it is an integral part of the plume (Fitton *et al.*, 1997; Thirlwall *et al.*, 2004) and may therefore be derived from recycled components and/or the lower mantle. This question is just as relevant for the CEG low-Ti basalts. Momme *et al.* (2006) argued that the CEG low-Ti basalts were derived from a distinct geographical location (i.e. within the newly developed oceanic rift), on the basis of (1) a lack of evidence for mixing of the CEG low- and high-Ti magmas, (2) concentration of the low-Ti lavas in coastal regions with decreasing abundances to the west, and (3) their main restriction to the boundary between the Milne Land and Geikie Plateau Formations. This could in turn imply that the CEG low-Ti magmas represent (1) melting of typical North Atlantic depleted MORB mantle in a newly developed rift zone, (2) lateral or radial zonation of the plume such that the low-Ti magma source was located preferentially below the rift zone (e.g. Søager & Holm, 2011), or (3) that the low-Ti sources were distributed as blobs throughout the plume, but were relatively refractory and began to melt only during the rapid thinning and decompression occurring in the rift zone.

In detail, the low-Ti lavas, although mainly concentrated at the top of the Milne Land Formation, are in fact distributed sporadically throughout the Plateau Basalt sequence (see Tegner *et al.*, 1998*a*). Furthermore, low-Ti and high-Ti lavas occur contemporaneously and some low-Ti eruption sites are found up to 50 km inland from the coast (L. M. Larsen, personal communication). This suggests that the low-Ti source was an integral part of the melting column.

Comparison with MORB

The ΔNb parameter [$=1{\cdot}72 + \log(Nb/Y) - 1{\cdot}92\log(Zr/Y)$], defined by Fitton *et al.* (1997), has been used to distinguish between Iceland plume and global N-MORB compositions, such that Icelandic magmas have $\Delta Nb > 0$ and N-MORB has $\Delta Nb < 0$. The low-Ti basalts plot below the Iceland field ($\Delta Nb < 0$) and overlap with compositions from the Reykjanes and Kolbeinsey Ridges (Fig. 11); contamination cannot explain this offset from Iceland. The Reykjanes data are filtered to include only data from 57–61°N and should thus not be excessively influenced by the Iceland plume, and plot consistently with $\Delta Nb < 0$. In contrast, the Kolbeinsey data come from immediately north of Iceland and spread across the Iceland–N-MORB boundary, consistent with significant influence from the plume. Only a single low-Ti sample plots within the Iceland field; this sample (412493) comes from stratigraphically higher in the Plateau Basalt sequence within the Skrænterne Formation. The high-Ti lavas plot within or close to the Iceland field ($\Delta Nb \sim 0$). Following the arguments of Fitton *et al.* (1997), the ΔNb values therefore suggest that the low-Ti basalts were derived from an N-MORB source, whereas the high-Ti magmas were derived from the Iceland plume, consistent with the model for CEG of Momme *et al.* (2006). The ΔNb systematics also suggests a closer link between the CEG low-Ti basalts and the ridges adjacent to Iceland, rather than Iceland itself. As discussed in more detail below, isotopic evidence suggests that most of the upper mantle in the North Atlantic is polluted by the Iceland plume and this complicates distinguishing between global N-MORB sources and upper mantle compositions in the North Atlantic.

The suitability of ΔNb to distinguish between N-MORB and Icelandic compositions has been questioned by Hanan *et al.* (2000) and Stracke *et al.* (2003). Those workers presented datasets in which the contrast between Iceland and MORB is less distinct, together with arguments

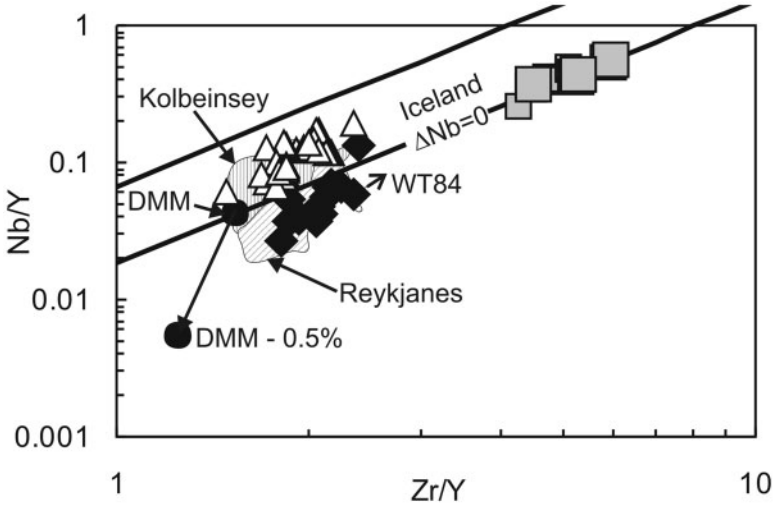

Fig. 11. Variation of Nb/Y vs Zr/Y showing the region ($\Delta Nb > 0$) considered to distinguish Iceland plume compositions from MORB ($\Delta Nb < 0$) (Fitton *et al.*, 2003). CEG data were obtained by XRF at Edinburgh University. The small arrow by the low-Ti data field represents a vector for 2% contamination by average crust (WT84) from Weaver & Tarney (1984). The source of the CEG low-Ti basalts must be more depleted than typical depleted MORB mantle (DMM; e.g. Workman & Hart, 2005), and a potential residual source composition (following removal of 0·5% melt in the spinel facies) is shown, calculated using aggregated non-modal melting as discussed in Fig. 8. Fields for Kolbeinsey are from Devey *et al.* (1994) and for Reykjanes from Murton *et al.* (2002). Data for Theistareykir (open triangles) are from Stracke *et al.* (2004); additional CEG high-Ti data (small squares) are from Andreasen *et al.* (2004).

suggesting that the parameter may also be affected by variable extents and pressures of melting. For example, the REE modelling presented above suggests that the source for the low-Ti basalts must be somewhat more depleted than a typical depleted upper mantle MORB source, and removal of only small degrees of melt is sufficient to shift the residual mantle source to negative ΔNb (see Fig. 11). In response to criticisms of the ΔNb parameter, Kempton *et al.* (2000) and Fitton *et al.* (2003) proposed that N-MORB and Iceland compositions can also be distinguished in Hf–Nd isotope space, where, at relatively radiogenic compositions, global N-MORB plots below the mantle reference line, and Icelandic and other NAIP compositions plot above the mantle reference line. Source-corrected Hf and Nd isotopic compositions for both the low-Ti and high-Ti CEG basalts fall within the Iceland field (Fig. 7), suggesting derivation from the Iceland plume rather than from depleted MORB mantle, and therefore contradict conclusions based on ΔNb systematics. The effect of crustal contamination on these distinctions is limited by a lack of Hf isotope data for potential crustal contaminants. However, Peate *et al.* (2003) showed that contamination in the Prinsen af Wales Bjerge formation results in a trend to less radiogenic compositions that largely parallels the mantle reference line. The small degrees of contamination indicated in the CEG low-Ti basalts are considered to be insufficient to change this apparent distinction from N-MORB.

Since 2003 considerably more new Hf isotope data have been published for North Atlantic MORB (see Fig. 7). These new data blur the original contrasts observed by Fitton *et al.* (2003). Most new data overlap with the suggested Iceland field, and only a subset of samples (from between the Equator and 35°N) plot below the mantle reference line to overlap with the Fitton *et al.* (2003) N-MORB field (Fig. 7). The Charlie–Gibbs Fracture Zone (~52°N) has been suggested as a major discontinuity in the North Atlantic, possibly representing the southern limit of influence of the Iceland plume (e.g. Mertz & Haase, 1997; Thirlwall *et al.*, 2004). All MORB samples north of here plot above the mantle reference line and overlap with the Iceland field, even when data are delineated with respect to depth (>2500 m below sea level) to minimize possible plume influences. The original data used by Fitton *et al.* (2003) to define global MORB came from the Pacific and Indian Oceans, as well as the Atlantic Ocean south of the Charlie–Gibbs Fracture Zone. New data, as compiled in Fig. 7, illustrate that North Atlantic MORB are distinct from global MORB in Hf–Nd space, but cannot be distinguished from Icelandic compositions. On this basis, it can be argued that the low-Ti basalts have Hf–Nd isotope compositions that distinguish them from typical global N-MORB mantle and non-plume affected Atlantic MORB (e.g. south of Charlie–Gibbs Fracture Zone), but they cannot be used on a more local scale to discriminate between Iceland plume and North Atlantic MORB compositions. This is perhaps not surprising and we consider it questionable that such material would have been preserved under CEG at the time of break-up. Plume-related magmatism was initiated under Greenland at least 6 Myr before the emplacement of the Plateau Basalts (61 Ma, Saunders *et al.*, 1997; Storey *et al.*,

2007) and it is likely that much of the upper mantle under Greenland was contaminated or eroded and replaced by plume material by the time of break-up, especially given the proposed size of the initial plume head (~2000 km in diameter).

Thirlwall *et al.* (2004) have argued that Iceland plume and North Atlantic MORB compositions can also be distinguished from global MORB by having negative Δ^{207}Pb and positive Δ^{208}Pb. Negative Δ^{207}Pb compositions around Iceland overlap spatially with a zone of elevated $^{3}He/^{4}He$ and are therefore considered to be a deep-mantle plume signature in the region (Thirlwall *et al.*, 2004). The ridges immediately surrounding Iceland also display negative Δ^{207}Pb and positive Δ^{208}Pb and have compositions distinct from MORB further south with more radiogenic Sr at a given $^{143}Nd/^{144}Nd$ or $^{206}Pb/^{204}Pb$. These distinctions are considered to represent contributions from the plume to ridges throughout the region.

Distinguishing between different ridge and plume components on Iceland is possible only by using precise double-spike Pb isotope data, as discussed in detail by Thirlwall *et al.* (2004). The low-Ti data presented here were produced using similar techniques and should be directly comparable (see Baker *et al.*, 2004). However, more precise comparison of the low-Ti lavas with depleted Iceland and adjacent ridge compositions is hampered by the inherent uncertainties induced by uncertainties in age corrections (see above) and crustal contamination. Maximum shifts in Pb isotopic composition owing to age correction are small compared with the spread in data and generally parallel the modern spread in compositions. Crustal contamination, in turn, shifts samples to more negative Δ^{207}Pb and more positive Δ^{208}Pb (Fig. 10).

It is apparent that the least contaminated CEG (and FI) low-Ti basalts also record the North Atlantic signature of negative Δ^{207}Pb and positive Δ^{208}Pb, and are distinct from Atlantic MORB south of the influence of the Iceland plume [e.g. data from 22–53°N of Thirlwall *et al.* (2004)]. Together with the Hf–Nd isotope systematics, these characteristics suggest a broad relationship between the low-Ti lavas and depleted components on Iceland and the surrounding ridges, but do not allow a definitive distinction between Iceland plume and North Atlantic MORB compositions.

Depleted compositions on and around Iceland are dominated by the IDl component to the north (Theistareykir and Kolbeinsey Ridge) and the RRDl component to the south (Reykjanes Ridge). These components are distinguished on the basis of higher $^{206}Pb/^{204}Pb$, more negative Δ^{207}Pb and less positive Δ^{208}Pb for the RRDl component (Thirlwall *et al.*, 2004). In plots of $^{206}Pb/^{204}Pb$ vs Δ^{207}Pb and Δ^{208}Pb, many of the CEG and FI low-Ti basalts plot close to both the IDl and RRDl components of Thirlwall *et al.* (2004) [which are in turn similar to the FDC component of Søager & Holm (2011)], with offsets to lower $^{206}Pb/^{204}Pb$ and Δ^{207}Pb and higher Δ^{208}Pb owing to small amounts of crustal contamination. In detail, the extension of ridge compositions and low-Ti CEG basalts to less radiogenic Sr and higher εNd than Theistareykir (Fig. 7), together with their negative ΔNb, suggests that the low-Ti basalts have closer affinities to ridge compositions (Kolbeinsey or Reykjanes) than depleted Iceland compositions such as Theistareykir. Furthermore, the somewhat higher $^{206}Pb/^{204}Pb$ coupled with a tendency towards somewhat less radiogenic $^{87}Sr/^{86}Sr$ in the low-Ti basalts suggests that they have a greater affinity to Reykjanes Ridge compositions (RRDl end-member) than those from Theistareykir and Kolbeinsey (IDl). Age or source correction issues cannot be used to argue for a closer affinity to an IDl parent as these will result in lower $^{87}Sr/^{86}Sr$ and $^{206}Pb/^{204}Pb$. The low-Ti basalts also have higher $^{87}Sr/^{86}Sr$ at a given $^{143}Nd/^{144}Nd$ than modern Atlantic MORB unaffected by the Iceland plume, features also observed in the Reykjanes and Kolbeinsey Ridges (Thirlwall *et al.*, 2004).

In summary, the available isotopic data indicate a close similarity between the CEG low-Ti basalts and depleted compositions on Iceland and adjacent ridges, and an apparent contrast with global MORB. The isotopic data suggest a closer affinity to ridges adjacent to Iceland, rather than depleted compositions on Iceland such as Theistareykir, in particular owing to the lower $^{87}Sr/^{86}Sr$ and higher $^{143}Nd/^{144}Nd$ and negative ΔNb of the CEG low-Ti basalts.

Comparison between CEG low-Ti lavas, N-MORB, Iceland and adjacent ridges: trace elements

Trace element systematics also provide constraints on further linking the CEG low-Ti basalts to depleted Iceland and/or adjacent ridge mantle components and distinguishing them from global MORB. The negative ΔNb of the CEG low-Ti basalts suggests a similarity to global MORB, and a distinction from Iceland, and is primarily a consequence of low Nb concentrations. Pollution of ridge segments immediately adjacent to the plume results in positive ΔNb. Negative ΔNb magmas are not so unusual in the NAIP and are also found pre-dating and contemporaneous with break-up in SE Greenland, in the upper part of the FI sequence, West Greenland and Baffin Island and throughout the British Palaeogene Igneous Province (Fitton *et al.*, 1997). However, the CEG low-Ti basalts also have trace element characteristics that clearly distinguish them from typical N-MORB; for example, their characteristic positive enrichments in Sr and Ba, generally depleted nature, and relatively low Nb and LREE concentrations compared with MREE when normalized

to average N-MORB (Fig. 5). Thus a typical global N-MORB source is not indicated for the CEG low-Ti basalts.

As noted previously, the low-Ti basalts also exhibit many trace element similarities to depleted magmas on Iceland such as Theistareykir, but are in detail distinguished by lower Nb, higher Zr, Hf, Th and U, and enrichments in Pb. Isotopic data suggest similarity to the ridges surrounding Iceland, yet more detailed trace elemental comparisons are hampered by a lack of comparative samples with full trace element analyses, difficulties in analysing low abundances of U, Th and Pb, and the potential effects of seawater alteration. Full trace element analyses of MORB compositions from the Reykjanes Ridge and the northern Kolbeinsey Ridge (71–72°N) were presented by Murton *et al*. (2002) and Haase *et al*. (2003) respectively. ICP-MS data from the Reykjanes Ridge show more enrichment in the HREE compared with the CEG low-Ti basalts, probably reflecting melting dominantly at shallow levels; the data exhibit highly variable Sr with both positive and negative anomalies (Fig. 12). The Reykjanes Ridge samples also show similar to lower concentrations of LREE, Rb, Ba, Nb and U compared with the CEG low-Ti basalts; however, the dataset is characterized by highly variable Pb concentrations (both positive and negative anomalies) and negative Th anomalies (Fig. 12). We suspect this reflects analytical difficulties in such low concentration samples rather than true magmatic signatures. A subset of samples analysed by isotope dilution by Murton *et al*. (2002) is similar to the CEG low-Ti samples in having positive Sr anomalies, yet these are distinct in that they show no positive Pb anomalies and have negative Th and positive U anomalies. The northern Kolbeinsey Ridge data exhibit a positive Sr anomaly similar to CEG and Iceland when normalized to MORB, but are otherwise clearly distinct from the CEG low-Ti basalts with respect to their trace element compositions and are enriched relative to N-MORB in Ba, Th, Nb, La and Ce (Fig. 12). No full published trace element analyses could be found for the Kolbeinsey Ridge closer to Iceland. The CEG low-Ti basalts appear to have similar Ba/La, Nb/Zr, Zr/Hf and La/Sm to the more depleted middle Kolbeinsey Ridge (68–

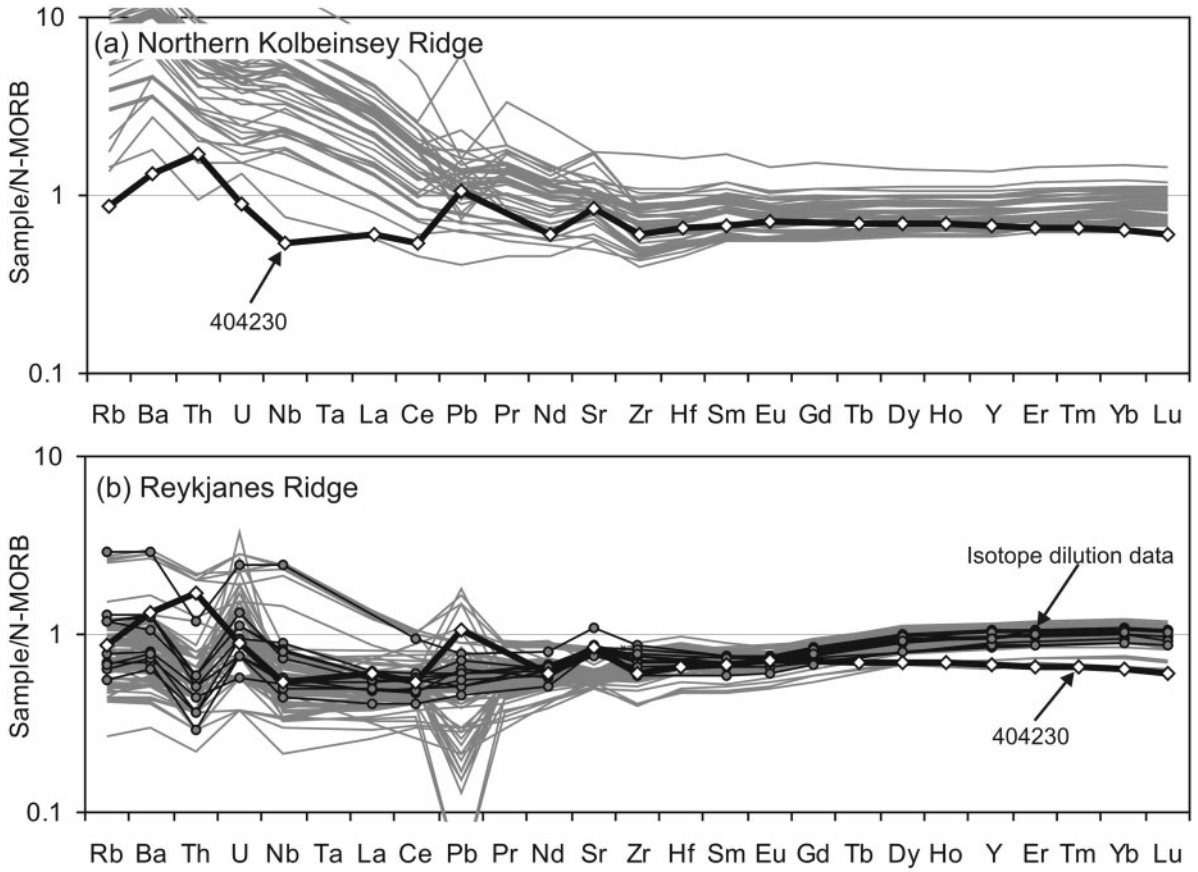

Fig. 12. N-MORB-normalized extended multi-element diagrams, normalized to the values of Arvelo & McDonough. (2010), comparing a representative CEG low-Ti lava (404230; bold black line, white diamonds) with the Northern Kolbeinsey Ridge (70·7–71·7°N) (Haase *et al*., 2003) and the Reykjanes Ridge (restricted to 61–57°N as samples north of here are enriched and influenced by the Iceland plume) (Murton *et al*. 2002); data from PetDB. Samples from the Reykjanes Ridge represented by black lines and grey circles are isotope dilution data.

71°N) based on data fields presented by Haase *et al.* (2003). On the basis of available trace element data, we therefore conclude that the CEG low-Ti basalts represent melts of a depleted source component that is similar to, but nevertheless subtly distinct from, that which produced the depleted magmatism on Iceland and adjacent ridges.

Origin of the depleted component(s)

Thirlwall *et al.* (2004) argued that the isotopic compositions of the various end-member components identified on Iceland can be attributed to the involvement of a recycled component of relatively young (Palaeozoic) oceanic crust and/or upper mantle. Enrichments in Sr and Ba (and Pb) in mantle-normalized trace element diagrams for depleted magmas and melt inclusions have been argued to represent involvement of a recycled oceanic crust gabbro component in Iceland and several other plume systems (e.g. Chauvel & Hémond, 2000; Sobolev *et al.*, 2000; Skovgaard *et al.*, 2001; Kent *et al.*, 2002; Huang & Frey, 2005; Kokfelt *et al.*, 2006; Stroncik & Devey, 2011). The former gabbroic material, present in the plume as eclogite, inherits its high Sr concentration from original plagioclase cumulates, and partially melts at greater depths than the surrounding peridotite. The resultant highly siliceous melts rise and react with the surrounding peridotite to form reactive pyroxenites. These pyroxenites then remelt, and contribute a plagioclase signature by mixing with normal peridotitic melts (Yaxley & Sobolev, 2007). The CEG low-Ti basalts do not show consistent positive Sr anomalies such as those of the Iceland basalts when normalized to primitive mantle (Fig. 4), but do show positive enrichments in Sr, Pb and Ba when normalized to N-MORB, features also seen, for example, in depleted magmas from the Galapagos (Stroncik & Devey, 2011) and Icelandic picrites (e.g. Kokfelt *et al.*, 2006). Stroncik & Devey (2011) have recently suggested that such enrichments are especially characteristic of depleted magmas from hotspots erupted close to a spreading ridge axis, an environment reminiscent of that of the CEG low-Ti magmas. In line with previous studies, we also suggest that the gabbroic portion of recycled oceanic crust was also involved in the source of the CEG low-Ti basalts.

The different plume components identified in the Iceland basalts appear to mix readily to produce a broad spectrum of compositions, although mixing can often be idealized as binary mixing between two (hybrid) end-members when examining geographically limited datasets (e.g. Thirlwall *et al.*, 2004; Peate *et al.*, 2009). Recent studies have suggested that this in part reflects progressive mixing of initial melts formed at depth from fertile, enriched components in the plume with later melts of less fertile, depleted components at shallower levels (e.g. Kokfelt *et al.*, 2006; Maclennan, 2008). This contrasts markedly with the CEG and FI magmatism where the enriched and depleted components appear to remain separate and undergo little mixing. This has led workers to suggest that the two magma suites were derived from chemically and spatially distinct source regions, implying a zoned plume (e.g. Søager & Holm, 2011). However, as suggested above, the high-Ti source may contribute to the low-Ti magmas, but decoupling between trace element and isotopic compositions occurred owing to previous depletion of the high-Ti source during deeper level melting.

The occurrence of low-Ti basalts dispersed (albeit irregularly) throughout the Plateau Basalt sequence, and identification of eruption sites distal to the site of rifting, suggests that the depleted low-Ti mantle source component was an integral part of the plume. In the Sortebrae section, the number of low-Ti flows increases towards the Blosseville Coast (Tegner *et al.*, 1998*a*). These flows are not present in the Scoresby Sund area, which is otherwise composed of the same four formations of high-Ti basalts, although thinner than at the Blosseville Coast (Larsen *et al.*, 1989). This indicates that the low-Ti source was not evenly distributed in the source of the NAIP flood basalt region at 55 Ma. This source material was probably present as blobs of relatively depleted material within a plume column dominated by more fertile, enriched components [the CEG high-Ti source(s)]. As previously suggested by Tegner *et al.* (1998*a*), magmatism was dominated by melting of the more fertile and enriched components beneath a relatively thick lithospheric lid to produce the high-Ti basalts, leaving a residue of relatively incompatible element depleted material and less fertile components, following processes similar to those proposed by Stroncik & Devey (2011). Conditions only rarely reached pressures and temperatures allowing sporadic melting of the depleted components, perhaps during intermittent periods of increased uplift and extension and/or pulsation of the plume flux (e.g. Ito, 2001). The development of a new oceanic rift zone resulted in rapid extension and thinning of the lithosphere and uplift of the plume head. This allowed melting of the more depleted components with little contribution from the previously exhausted, more enriched components (Fig. 13).

As a final note we observe that many of the characteristic signatures of the CEG low-Ti basalts (low-Ti, depleted LREE, $\Delta Nd < 0$, depleted isotopic signatures, negative $\Delta^{207}Pb$ and positive $\Delta^{208}Pb$) are also observed in portions of the earlier magmatism associated with the initial impact of the Iceland plume, such as the Vaigat and Maligât Formations in West Greenland (Larsen & Pedersen, 2009) and depleted N-type lavas from Baffin Island (Stuart *et al.*, 2003; Kent *et al.*, 2004). In both cases, these depleted lavas are considered to be derived from a depleted, MORB-like upper mantle source, although more recently the Baffin Island magmas have been used as evidence for the preservation

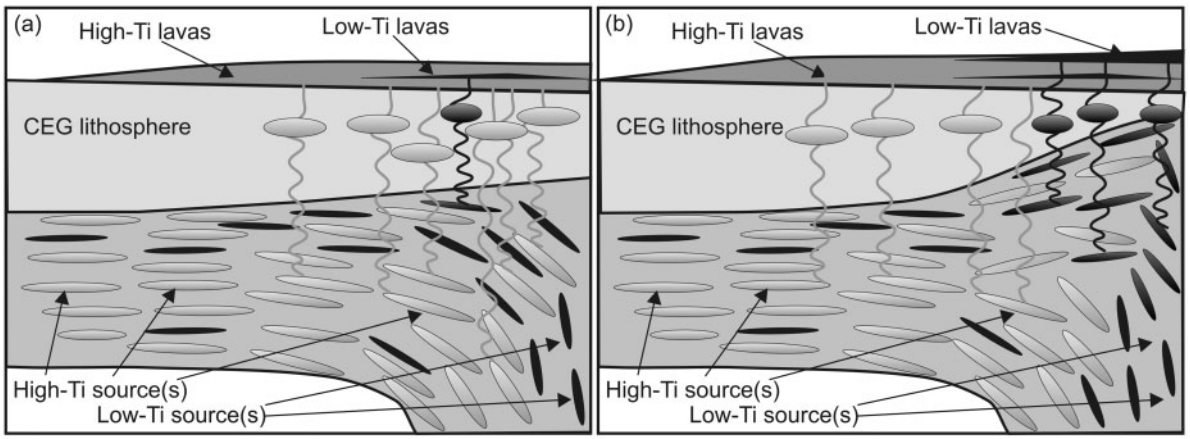

Fig. 13. Schematic model of the proto-Iceland plume under CEG [modified from Momme *et al.* (2002) and Søager & Holm (2011)]. (a) Prior to major lithospheric thinning, magmatism is dominated by melting of the high-Ti source(s) under a relatively thick lithospheric lid. (b) During lithospheric thinning, the low-Ti source(s) dominate melting in the region of thinning, with little contribution from the previously melt-depleted high-Ti source(s). Regional geology (i.e. increasing abundance of low-Ti lavas towards the coast) suggests that the low-Ti source was mostly concentrated towards the centre of rifting.

of a reservoir in the mantle from *c.* 4·5 billion years ago (Jackson *et al.*, 2010). The similarity of the Baffin Island, West Greenland, CEG low-Ti and modern Iceland depleted basalt geochemistry suggests the involvement of similar sources throughout the history of the Iceland plume. Our geochemical results indicate that the depleted component of the Iceland plume at 55 Ma bears many similarities to the depleted components today, but in detail is subtly distinct, potentially reflecting small variations in the age and composition of the recycled components with time (see also Barker *et al.*, 2006).

CONCLUSIONS

Sr, Nd, Pb and Hf isotope and trace element data for depleted low-Ti lavas from CEG suggest that they are derived from a depleted mantle component similar but not identical to that currently melting beneath Iceland and adjacent ridges, and clearly distinct from the source of the contemporaneous high-Ti magmas. The variations in trace element and isotopic compositions can be attributed to inputs from two depleted mantle sources, one of which is similar to the FDC component identified in the Faroe Islands, ridge components adjacent to Iceland (e.g. Reykjanes and Kolbeinsey Ridges) and depleted compositions in the Iceland plume as seen at Theistareykir (e.g. ID1). The other less-depleted component is isotopically similar to the high-Ti lavas. Small amounts (generally <1%) of contamination by amphibolitic and granulitic crustal components can be identified and cause scatter to higher $^{87}Sr/^{86}Sr$ and $\Delta^{208}Pb$, and lower $^{206}Pb/^{204}Pb$, εNd, εHf and $\Delta^{207}Pb$. The basalts have many isotopic and trace elemental characteristics in common with modern-day depleted compositions on Iceland (e.g. Theistareykir) and surrounding ridges. Although Nb–Zr–Y systematics suggest a MORB mantle source, the low-Ti CEG lavas, like the depleted components on Iceland, can be distinguished from global MORB by having negative $\Delta^{207}Pb$ and positive $\Delta^{208}Pb$, as well as relative enrichments in Ba, Sr and Pb. These enrichments suggest the involvement of a relatively young recycled, potentially gabbroic, oceanic crust component that is an integral part of the mantle plume. However, subtle differences between depleted compositions erupted at 55 Ma and today indicate that the depleted component has changed slightly with time. The main pulse of depleted magmatism appears to coincide with the onset of rifting, suggesting that these depleted components were able to generate significant volumes of melt only during the rapid uplift and extension associated with continental break-up. Lack of mixing between the high-Ti and low-Ti components may be due to prior depletion of the enriched components during melting at deeper levels.

ACKNOWLEDGEMENTS

We would like to thank David Ulfbeck for assistance in the Axiom MC-ICP-MS laboratory. Lotte Larsen is thanked for discussions on East Greenland geology and an informal review of the paper. Adrian Finch, Christian Tegner and an anonymous reviewer are also thanked for their constructive reviews. We thank Hans Christian Larsen for his support and leadership at the Danish Lithosphere Centre.

FUNDING

This study was initiated under the auspices of the now defunct Danish Lithosphere Centre, which was funded by the Danish National Research Foundation.

SUPPLEMENTARY DATA

Supplementary data for this paper are available at *Journal of Petrology* online.

REFERENCES

Agranier, A., Blichert-Toft, J., Graham, D., Debaille, V., Schiano, P. & Albarède, F. (2005). The spectra of isotopic heterogeneities along the mid-Atlantic Ridge. *Earth and Planetary Science Letters* **238**, 96–109.

Anders, E. & Grevesse, N. (1989). Abundances of the elements—meteoritic and solar. *Geochemica et Cosmochimica Acta* **53**, 197–214.

Andreasen, R., Peate, D. W. & Brooks, C. K. (2004). Magma plumbing systems in large igneous provinces: Inferences from cyclical variations in Palaeogene East Greenland basalts. *Contributions to Mineralogy and Petrology* **147**, 438–452.

Andres, M., Blichert-Toft, J. & Schilling, J.-G. (2004). Nature of the depleted upper mantle beneath the Atlantic: evidence from Hf isotopes in normal mid-ocean ridge basalts from 79°N to 55°S. *Earth and Planetary Science Letters* **225**, 89–103.

Arevalo, R., Jr & McDonough, W. F. (2010). Chemical variation and regional diversity observed in MORB. *Chemical Geology* **271**, 70–85.

Baker, J. A., Menzies, M. A., Thirlwall, M. F. & Macpherson, C. G. (1997). Petrogenesis of Quaternary intraplate volcanism, Sana'a, Yemen: implications for plume–lithosphere interaction and polybaric melt hybridization. *Journal of Petrology* **38**, 1359–1390.

Baker, J., Waight, T. & Ulfbeck, D. (2002). Rapid and highly reproducible analysis of rare earth elements by multiple collector inductively coupled plasma mass spectrometry. *Geochimica et Cosmochimica Acta* **66**, 3635–3643.

Baker, J., Peate, D. W., Waight, T. & Meyzen, C. (2004). Pb isotopic analysis of standards and samples using a ^{207}Pb–^{204}Pb double spike and thallium to correct for mass bias with a double focusing MC-ICP-MS. *Chemical Geology* **211**, 275–303.

Barker, A. K. (2006). Trace elements and isotope constraints on mantle sources and processes in North Atlantic and Cape Verde magmatism, PhD thesis, University of Copenhagen.

Barker, A. K., Baker, J. A. & Peate, D. W. (2006). Interaction of the rifting East Greenland margin with a zoned ancestral Iceland plume. *Geology* **34**, 481–484.

Blichert-Toft, J. & White, W. M. (2001). Hf isotope geochemistry of the Galapagos Islands. *Geochemistry, Geophysics, Geosystems* **2**, doi:10.1029/2000GC000138.

Blichert-Toft, J., Agranier, A., Andres, M., Kingsley, R., Schilling, J.-G. & Albarède, F. (2005). Geochemical segmentation of the Mid-Atlantic Ridge north of Iceland and ridge–hot spot interaction in the North Atlantic. *Geochemistry, Geophysics, Geosystems* **6**, doi:10.1029/2004GC000788.

Brooks, C. K. (2012). *The East Greenland rifted volcanic margin. Geological Survey of Denmark and Greenland Bulletin* **24**, 1–96.

Chauvel, C. & Hémond, C. (2000). Melting of a complete section of oceanic crust: trace element and Pb isotopic evidence from Iceland. *Geochemistry, Geophysics, Geosystems* **1**, doi:10.1029/1999GC000002.

Debaille, V., Blichert-Toft, J., Agranier, A., Doucelance, R., Schiano, P. & Albarède, F. (2006). Geochemical component relationships in MORB from the Mid-Atlantic Ridge, 22–35°N. *Earth and Planetary Science Letters* **241**, 844–862.

Devey, C. W., Garbe-Schonberg, C. D., Stoffers, P., Chauvel, C. & Mertz, D. F. (1994). Geochemical effects of dynamic melting beneath ridges—reconciling major and trace element variations in Kolbeinsey (and global) mid-ocean ridge basalt. *Journal of Geophysical Research* **99**, 9077–9095.

Dickin, A. P. (1981). Isotope geochemistry of Tertiary igneous rocks from the Isle of Skye, N. W. Scotland. *Journal of Petrology* **22**, 155–189.

Ellam, R. M. & Stuart, F. M. (2000). The sub-lithospheric source of North Atlantic basalts: evidence for, and significance of, a common end-member. *Journal of Petrology* **41**, 919–932.

Fitton, J. G., Saunders, A. D., Norry, M. J., Hardarson, B. S. & Taylor, R. N. (1997). Thermal and chemical structure of the Iceland plume. *Earth and Planetary Science Letters* **153**, 197–208.

Fitton, J. G., Saunders, A. D., Larsen, L. M., Hardarson, B. S. & Norry, M. J. (1998). Volcanic rocks from the southeast Greenland margin at 63°N: composition, petrogenesis and mantle sources. In: Saunders, A. D., Larsen, H. C. & Wise, S. W., Jr (eds) *Proceedings of the Ocean Drilling Program, Scientific Results, 152*. College Station, TX: Ocean Drilling Program, pp. 331–350.

Fitton, J. G., Larsen, L. M., Saunders, A. D., Hardarson, B. S. & Kempton, P. D. (2000). Palaeogene continental to oceanic magmatism on the SE Greenland continental margin at 63°N: a review of the results of Ocean Drilling Program Legs 152 and 163. *Journal of Petrology* **41**, 951–966.

Fitton, J. G., Saunders, A. D., Kempton, P. D. & Hardarson, B. S. (2003). Does depleted mantle form an intrinsic part of the Iceland plume? *Geochemistry, Geophysics, Geosystems* **4**, doi:10.1029/2002GC000424.

Fram, M. S. & Lesher, C. E. (1997). Generation and polybaric differentiation of East Greenland early Tertiary flood basalts. *Journal of Petrology* **38**, 231–275.

Frey, F. A., Huang, S., Blichert-Toft, J., Regelous, M. & Boyet, M. (2005). Origin of depleted components in basalt related to the Hawaiian hot spot: Evidence from isotopic and incompatible element ratios. *Geochemistry, Geophysics, Geosystems* **6**, doi:10.1029/2004GC000757.

Haase, K. M., Devey, C. W. & Wieneke, M. (2003). Magmatic processes and mantle heterogeneity beneath the slow-spreading northern Kolbeinsey Ridge segment, North Atlantic. *Contributions to Mineralogy and Petrology* **144**, 428–448.

Hanan, B. B. & Schilling, J.-G. (1997). The dynamic evolution of the Iceland mantle plume: the lead isotope perspective. *Earth and Planetary Science Letters* **151**, 43–60.

Hanan, B. B., Blichert-Toft, J., Kingsley, R. & Schilling, J.-G. (2000). Depleted Iceland mantle plume geochemical signature: artifact of multicomponent mixing? *Geochemistry, Geophysics, Geosystems*, **1**, doi:10.1029/1999GC000009.

Hansen, H. & Nielsen, T. F. D. (1999). Crustal contamination in Palaeogene East Greenland flood basalts: plumbing system evolution during continental rifting. *Chemical Geology* **157**, 89–118.

Hart, S. R. (1984). A large scale isotope anomaly in the southern Hemisphere mantle. *Nature* **309**, 753–757.

Hoernle, K., Werner, R., Morgan, J. P., Garbe-Schonberg, D., Bryce, J. & Mrazek, J. (2000). Existence of complex spatial zonation in the Galapagos plume for at least 14 m.y. *Geology* **28**, 435–438.

Holm, P. M., Hald, N. & Waagstein, R. (2001). Geochemical and Pb–Sr–Nd isotopic evidence for separate hot depleted and Iceland plume mantle sources for the Paleogene basalts of the Faroe Islands. *Chemical Geology* **178**, 95–125.

Huang, S. & Frey, F. A. (2005). Recycled oceanic crust in the Hawaiian Plume: evidence from temporal geochemical variations within the Koolau Shield. *Contributions to Mineralogy and Petrology* **149**, 556–575.

Huppert, H. E. & Sparks, R. S. J. (1985). Cooling and contamination of mafic and ultramafic magmas during ascent through continental crust. *Earth and Planetary Science Letters* **74**, 371–386.

Ito, G. (2001). Reykjanes 'V'-shaped ridges originating from a pulsing and dehydrating mantle plume. *Nature* **411**, 681–684.

Jackson, M. G., Carlson, R. W., Kurz, M. D., Kempton, P. D., Francis, D. & Blusztajn, J. (2010). Evidence for the survival of the oldest terrestrial mantle reservoir. *Nature* **466**, 853–856.

Johnson, C. M. & Beard, B. L. (1993). Evidence from hafnium isotopes for ancient sub-oceanic mantle beneath the Rio Grande rift. *Nature* **362**, 441–444.

Kalsbeek, F., Austrheim, H., Bridgwater, D., Hansen, B. T., Pedersen, S. & Taylor, P. N. (1993). Geochronology of Archean and Proterozoic events in the Ammassalik area, south-east Greenland, and comparison with the Lewisian of Scotland and the Nagssugtoqidian of west Greenland. *Precambrian Research* **62**, 239–270.

Kempton, P. D., Fitton, J. G., Saunders, A. D., Nowell, G. M., Taylor, R. N., Hardarson, B. S. & Pearson, G. (2000). The Iceland plume in space and time: a Sr–Nd–Pb–Hf study of the North Atlantic rifted margin. *Earth and Planetary Science Letters* **177**, 255–271.

Kent, A. J. R., Baker, J. A. & Weidenbeck, M. (2002). Contamination and melt aggregation processes in continental flood basalts: constraints from melt inclusions in Oligocene basalt from Yemen. *Earth and Planetary Science Letters* **202**, 577–594.

Kent, A. J. R., Stolper, E. M., Francis, D., Woodhead, J., Frei, R. & Eiler, J. (2004). Mantle heterogeneity during the formation of the North Atlantic Igneous Province: Constraints from trace element and Sr–Nd–Os–O isotope systematics of Baffin Island picrites. *Geochemistry, Geophysics, Geosystems* **5**, doi:10.1029/2004GC000743.

Kitagawa, H., Kobayashi, K., Makishima, A. & Nakamura, E. (2008). Multiple pulses of the mantle plume: Evidence from Tertiary Icelandic lavas. *Journal of Petrology* **49**, 1365–1396.

Kokfelt, T. F., Hoernle, K., Hauff, F., Fiebig, J., Werner, R. & Garbe-Schonberg, D. (2006). Combined trace element and Pb–Nd–Sr–O isotope evidence for recycled oceanic crust (upper and lower) in the Iceland mantle plume. *Journal of Petrology* **47**, 1705–1749.

Kystol, J. & Larsen, L. M. (1999). Analytical procedures in the Rock Geochemical Laboratory of the Geological Survey of Denmark and Greenland. *Geology of Greenland Survey Bulletin* **184**, 59–62.

Larsen, H. C. & Saunders, A. D. (1998). Tectonism and volcanism at the southeast Greenland rifted margin: a record of plume impact and later continental rupture. In: Saunders, A. D., Larsen, H. C. & Wise, S. W., Jr (eds) *Proceedings of the Ocean Drilling Program, Scientific Results, 152*. College Station, TX: Ocean Drilling Program, pp. 503–533.

Larsen, L. M. & Pedersen, A. K. (2009). Petrology of the Paleocene picrites and flood basalts on Disko and Nuusuaq, West Greenland. *Journal of Petrology* **50**, 1667–1711.

Larsen, L. M. & Watt, W. S. (1985). Episodic volcanism during break-up of the North-Atlantic—evidence from the East Greenland plateau basalts. *Earth and Planetary Science Letters* **73**, 105–116.

Larsen, L. M., Watt, W. S. & Watt, M. (1989). Geology and petrology of the lower Tertiary plateau basalts of the Scoresby Sund region, East Greenland. *Grønlands Geologiske Undersøgelse Bulletin* **157**, 1–164.

Larsen, L. M., Waagstein, R., Pedersen, A. K. & Storey, M. (1999). Trans-Atlantic correlation of the Palaeogene volcanic successions in the Faroe Islands and East Greenland. *Journal of the Geological Society, London* **156**, 1081–1095.

Le Bas, M. J. (2000). IUGS reclassification of the high-Mg and picritic volcanic rocks. *Journal of Petrology* **41**, 1467–1470.

Leeman, W. P., Dacsch, E. J. & Kays, M. A. (1976). $^{207}Pb/^{206}Pb$ whole-rock age of gneisses from the Kangerdlugssuaq area, eastern Greenland. *Nature* **263**, 469–471.

Luais, B., Telouk, P. & Albarède, F. (1997). Precise and accurate neodymium isotopic measurements by plasma-source mass spectrometry. *Geochimica et Cosmochimica Acta* **61**, 4847–4854.

Maclennan, J. (2008). Lead isotope variability in olivine-hosted melt inclusions from Iceland. *Geochimica et Cosmochimica Acta* **72**, 4159–4176.

McCoy-West, A. J., Baker, A. J., Faure, K. & Wysoczanski, R. (2010). Petrogenesis and origins of mid-Cretaceous continental intraplate volcanism in Marlborough, New Zealand: implications for the long-lived HIMU magmatic mega-province of the SW Pacific. *Journal of Petrology* **51**, 2003–2045.

McDonough, W. F. & Sun, S.-S. (1995). The composition of the Earth. *Chemical Geology* **120**, 223–253.

Mertz, D. F. & Haase, K. M. (1997). The radiogenic isotope composition of the high-latitude North Atlantic mantle. *Geology* **25**, 411–414.

Momme, P., Tegner, C., Brooks, C. K. & Keays, R. R. (2002). The behaviour of platinum-group elements in basalts from the East Greenland rifted margin. *Contributions to Mineralogy and Petrology* **143**, 133–153.

Momme, P., Tegner, C., Brooks, C. K. & Keays, R. R. (2006). Two melting regimes during Paleogene flood basalt generation in East Greenland: combined REE and PGE modelling. *Contributions to Mineralogy and Petrology* **151**, 88–100.

Murton, B. J., Taylor, R. N. & Thirlwall, M. T. (2002). Plume–ridge interaction: a geochemical perspective from the Reykjanes Ridge. *Journal of Petrology* **43**, 1987–2012.

Neuhoff, P. S., Watt, W. S., Bird, D. K. & Pedersen, A. K. (1997). Timing and structural relations of regional zeolite zones in basalts of the East Greenland continental margin. *Geology* **25**, 803–806.

Peate, D. W. & Stecher, O. (2003). Isotopic evidence for contributions from different Iceland mantle components to Palaeogene East Greenland flood basalts. *Lithos* **67**, 39–52.

Peate, D. W., Baker, J. A., Blichert-Toft, J., Hilton, D. R., Storey, M., Kent, A. J. R., Brooks, C. K., Hansen, H., Pedersen, A. K. & Duncan, R. A. (2003). The Prinsen af Wales Bjerge Formation lavas, East Greenland: the transition from tholeiitic to alkalic magmatism during Palaeogene continental break-up. *Journal of Petrology* **44**, 279–304.

Peate, D. W., Barker, A. K., Riishuus, M. S. & Andreasen, R. (2008). Temporal variations in crustal assimilation of magma suites in the East Greenland flood basalt province: Tracking the evolution of magmatic plumbing systems. *Lithos* **102**, 179–197.

Peate, D. W., Baker, J. A., Jakobsson, S. P., Waight, T. E., Kent, A. J. R., Grassineau, N. V. & Skovgaard, A. C. (2009). Historic magmatism on the Reykjanes Peninsula, Iceland: a snap-shot of melt generation at a ridge segment. *Contributions to Mineralogy and Petrology* **157**, 359–382.

Peate, D. W., Breddam, K., Baker, J. A., Kurz, M., Barker, A. K., Prestvik, T., Grassineau, N. & Skovgaard, A. C. (2010). Compositional characteristics and spatial distribution of enriched Icelandic mantle components. *Journal of Petrology* **51**, 1447–1475.

Pedersen, A. K., Watt, M., Watt, W. S. & Larsen, L. M. (1997). Structure and stratigraphy of the Early Tertiary basalts of the Blosseville Kyst, East Greenland. *Journal of the Geological Society, London* **154**, 565–570.

Reiners, P. W., Nelson, B. K. & Ghiorso, M. S. (1995). Assimilation of felsic crust by basaltic magma: thermal limits and extents of crustal contamination of mantle-derived magmas. *Geology* **23**, 563–566.

Riishuus, M. S., Peate, D. W., Tegner, C., Wilson, J. R., Brooks, C. K. & Waight, T. E. (2005). Petrogenesis of syenites at a rifted continental margin: origin, contamination and interaction of alkaline mafic and felsic magmas in the Astrophyllite Bay Complex, East Greenland. *Contributions to Mineralogy and Petrology* **149**, 350–371.

Salters, V. J. M. & Stracke, A. (2004). Composition of the depleted mantle. *Geochemistry, Geophysics, Geosystems* **5**, doi:10.1029/2003GC000597.

Salters, V. J. M. & White, W. M. (1998). Hf isotope constraints on mantle evolution. *Chemical Geology* **145**, 447–460.

Saunders, A. D., Fitton, J. G., Kerr, A. C., Norry, M. J. & Kent, R. W. (1997). The North Atlantic Igneous Province. In: Mahoney, J. J. & Coffin, M. L. (eds) *Geophysical Monograph, American Geophysical Union* **100**, 45–93.

Shaw, D. M. (1970). Trace element fractionation during anatexis. *Geochimica et Cosmochimica Acta* **34**, 237–243.

Skovgaard, A. C., Storey, M., Baker, J., Blusztajn, J. & Hart, S. R. (2001). Osmium–oxygen isotopic evidence for a recycled and strongly depleted component in the Iceland mantle plume. *Earth and Planetary Science Letters* **194**, 259–275.

Søager, N. & Holm, P. M. (2009). Extended correlation of the Paleogene Faroe Islands and East Greenland plateau basalts. *Lithos* **107**, 205–215.

Søager, N. & Holm, P. M. (2011). Changing compositions in the Iceland plume; Isotopic and elemental constraints from the Paleogene Faroe flood basalts. *Chemical Geology* **280**, 297–313.

Sobolev, A. V., Hofmann, A. W. & Nikogoslan, I. K. (2000). Recycled oceanic crust observed in 'ghost plagioclase' within the source of Mauna Loa lavas. *Nature* **404**, 989–990.

Storey, M., Duncan, R. A. & Tegner, C. T. (2007). Timing and duration of volcanism in the North Atlantic Igneous Province: Implications for geodynamics and links to the Iceland hotspot. *Chemical Geology* **241**, 264–281.

Stracke, A. & Bourdon, B. (2009). The importance of melt extraction for tracing mantle heterogeneity. *Geochimica et Cosmochimica Acta* **73**, 218–238.

Stracke, A., Zindler, A., Salters, V. J. M., McKenzie, D., Blichert-Toft, J., Albarède, F. & Gronvold, K. (2003). Theistareykir revisited. *Geochemistry, Geophysics, Geosystems* **4**, doi:10.1029/2001GC000201.

Stroncik, N. A. & Devey, C. W. (2011). Recycled gabbro signature in hotspot magmas unveiled by plume–ridge interactions. *Nature Geoscience* **4**, 393–397.

Stuart, F. M., Lass-Evans, S., Fitton, J. G. & Ellam, R. M. (2003). High He-3/He-4 ratios in picritic basalts from Baffin Island and the role of a mixed reservoir in mantle plumes. *Nature* **424**, 57–59.

Taylor, P. N., Kalsbeek, F. & Bridgwater, D. (1992). Discrepancies between neodymium, lead and strontium model ages from the Precambrian of southern east Greenland—evidence for a Proterozoic granulite-facies event affecting Archean gneisses. *Chemical Geology* **94**, 281–291.

Tegner, C., Lesher, C. E., Larsen, L. M. & Watt, W. S. (1998*a*). Evidence from the rare-earth-element record of mantle melting for cooling of the Tertiary Iceland plume. *Nature* **395**, 591–594.

Tegner, C., Duncan, R. A., Bernstein, S., Brooks, C. K., Bird, D. K. & Storey, M. (1998*b*). ^{40}Ar–^{39}Ar geochronology of Tertiary mafic intrusions along the East Greenland rifted margin: relation to flood basalts and the Iceland hotspot track. *Earth and Planetary Science Letters* **156**, 75–88.

Thirlwall, M. F., Upton, B. G. J. & Jenkins, C. (1994). Interaction between continental lithosphere and the Iceland plume: Sr–Nd–Pb isotope geochemistry of Tertiary basalts, NE Greenland. *Journal of Petrology* **35**, 839–879.

Thirlwall, M. F., Singer, B. S. & Marriner, G. F. (2000). ^{39}Ar–^{40}Ar ages and geochemistry of the basaltic shield stage of Tenerife, Canary Islands, Spain. *Journal of Volcanology and Geothermal Research* **103**, 247–297.

Thirlwall, M. F., Gee, M. A. M., Taylor, R. N. & Murton, B. J. (2004). Mantle components in Iceland and adjacent ridges investigated using double-spike Pb isotope ratios. *Geochimica et Cosmochimica Acta* **68**, 361–386.

Ulfbeck, D. G., Baker, J. A., Waight, T. E. & Krogstad, E. J. (2003). Rapid sample digestion by fusion and chemical separation of Hf for isotopic analysis. *Talanta* **59**, 365–373.

Waight, T. E., Baker, J. A. & Peate, D. W. (2002). Sr isotope ratio measurements by double focusing MC-ICPMS: techniques, observations and pitfalls. *International Journal of Mass Spectrometry* **221**, 229–244.

Weaver, B. L. & Tarney, J. (1981). Lewisian gneiss geochemistry and Archean crustal development models. *Earth and Planetary Science Letters* **55**, 171–180.

Weaver, B. & Tarney, J. (1984). Empirical approach to estimating the composition of the continental crust. *Nature* **310**, 575–577.

Wedepohl, K. H., Heinrichs, H. & Bridgwater, D. (1991). Chemical characteristics and genesis of the quartz–feldspathic rocks in the Archean crust of Greenland. *Contributions to Mineralogy and Petrology* **107**, 163–179.

Workman, R. K. & Hart, S. R. (2005). Major and trace element composition of the depleted MORB mantle (DMM). *Earth and Planetary Science Letters* **231**, 53–72.

Yaxley, G. M. & Sobolev, A. V. (2007). High-pressure partial melting of gabbro and its role in the Hawaiian magma source. *Contributions to Mineralogy and Petrology* **154**, 371–383.